

THE CHEMICAL COMPOSITIONS AND EVOLUTIONARY STATUS OF RED GIANTS IN THE OPEN CLUSTER NGC 6940

G. Böcek Topcu^{1*}, M. Afşar¹, , C. Sneden²

¹*Department of Astronomy and Space Sciences, Ege University, 35100 Bornova, İzmir, Turkey;*

²*Department of Astronomy and McDonald Observatory, The University of Texas, Austin, TX 78712*

Published 08 August 2016

ABSTRACT

We present the high resolution ($R \approx 60\,000$), high signal-to-noise ($S/N \simeq 120$) spectroscopic analysis of 12 red giant members of the Galactic open cluster NGC 6940. We applied Yonsei-Yale isochrones to the colour-magnitude diagram, which suggested an age of 1.1 Gyr for the cluster with a turn-off mass of $2\,M_{\odot}$. Atmospheric parameters (T_{eff} , $\log g$, $[\text{Fe}/\text{H}]$ and ξ_t) were determined via equivalent widths of Fe I, Fe II, Ti I, and Ti II lines. Calculated mean metallicity of the cluster is $\langle[\text{Fe}/\text{H}]\rangle = 0.04 \pm 0.02$. We derived abundances of α (Mg, Si, Ca), Fe-group (Sc, Ti, V, Cr, Mn, Fe, Co, Ni, Cu, Zn), and n -capture (Y, La, Nd, Eu) elements to be about solar. Light odd- Z elements Na and Al are slightly enhanced in MMU 108 and MMU 152 by ~ 0.34 dex and ~ 0.16 dex, respectively. Abundances of light elements Li, C, N, O, and $^{12}\text{C}/^{13}\text{C}$ ratios were derived from spectrum syntheses of the Li I resonance doublet at 6707 Å, [O I] line at 6300 Å, C₂ Swan bandheads at 5164 Å and 5635 Å, and strong $^{12,13}\text{CN}$ system lines in the 7995–8040 Å region. Most carbon isotopic ratios are similar to those found in other solar-metallicity giants, but MMU 152 has an unusual value of $^{12}\text{C}/^{13}\text{C} = 6$. Evaluation of the LiCNO abundances and $^{12}\text{C}/^{13}\text{C}$ ratios along with the present theoretical models suggests that all the red giants in our sample are core-helium-burning clump stars.

Key words: stars: abundances – stars: atmospheres. Galaxy: open clusters and associations: individual: NGC 6940

1 INTRODUCTION

Open star clusters give us important clues to help solve remaining puzzles of stellar evolution. Classical star cluster formation theories assume that members of individual open clusters (OCs) were formed from the same chemically homogeneous molecular cloud at the same time. This constraint yields numerous advantages for studies of both stellar and Galactic disc evolution. Since we can estimate cluster member stars' ages, masses, metallicities and reddening parameters more reliably than for field stars, we can analyze their model atmospheres and surface abundances more accurately. These data, in turn, lead to better determination of cluster member evolutionary status. In particular, precise positions

of red giants (RG)¹ in the color-magnitude diagram (CMD) along with the accurate abundances of their light elements involved in hydrogen burning (Li, C, N, O, $^{12}\text{C}/^{13}\text{C}$) can help us to differentiate the life stories of evolved cluster stars.

In standard stellar evolutionary theories, during the evolution from the main sequence to the tip of the RG branch the only mechanism that changes the surface abundances is so-called first-dredge up. The convective envelope movement of red giant branch (RGB) stars carries CN-cycle nuclear processed material to the surface. This results in depletion in the abundances of Li and C, increase in N abundance, and a drop in the $^{12}\text{C}/^{13}\text{C}$ ratio from initial values of about 90 on the main sequence to about 20–30 (e.g. Iben 1967; Dearborn et al. 1976).

¹ In this paper we will use the term red giant (RG) generically, meaning all cool and luminous stars; RGB will designate stars on the first ascent of the giant branch; and RC will designate He-burning red clump stars.

* E-mail: gamzebocek@gmail.com (GBT); melike.afsar@ege.edu.tr (MA); chris@verdi.as.utexas.edu (CS)

Table 1. NGC 6940 and Hyades cluster parameters.

Quantity	NGC 6940	Hyades
Right Ascension (2000) ^a	20 34 26	04 26 54
Declination (2000) ^a	+28 17 00	+15 52 00
Galactic longitude	69.860	180.064
Galactic latitude	-7.147	-22.343
Distance (pc)	770 ^c	45 ^d
$E(B - V)$ ^b	0.214	0.01
$(m - M)$	10.08 ^c	3.30 ^a
log Age	8.86	8.90

^a From the WEBDA database.^b Loktin et al. (2001)^c Kharchenko et al. (2005)^d Malysheva (1997)

The outline of this chemical evolution from the main sequence to the RG domain is qualitatively well understood; chemical composition studies of field and OC stars confirm the predicted surface abundance changes. However, there are significant remaining puzzles. For example, consider the $^{12}\text{C}/^{13}\text{C}$ ratio. This is one of the most useful tracers of stellar evolution stages; it is predicted well by theory and easy to determine observationally. However it has been long known that many RGs in the field and in open or globular clusters have $^{12}\text{C}/^{13}\text{C} < 20$ (e.g., Day et al. 1973; Tomkin et al. 1976; Lambert & Ries 1981; Gilroy 1989; Gilroy & Brown 1991; Luck 1994; Tautvaišienė et al. 2000; Tautvaišienė et al. 2001, 2005; Smiljanic et al. 2009; Mikolaitis et al. 2010, 2011b,a, 2012). The isotopic ratios of some RGs even approach the CN-cycle equilibrium value of $^{12}\text{C}/^{13}\text{C} = 3-4$ (Caughlan 1965). These low values are clear signs of further mixing and/or significant mass loss that is not accounted for by the classical stellar evolution theories. The elemental abundances of other CN-cycle participants often are also at odds with predictions. The source/theory/mechanism(s) of the extra-mixing is an ongoing discussion.

To better understand the discrepancy between classical theories and observations in evolving stars, there is increasing attention to high-resolution spectroscopic studies of RGs in OCs. Several groups are increasing the knowledge in this field; e.g. Drazdauskas et al. (2016); Reddy & Lambert (2016); Smiljanic et al. (2016), and references therein. For nearly two decades the WIYN Open Cluster Study² (eg. Mathieu 2000) group has systematically investigated the photometric and spectroscopic properties of OCs. Renewed efforts on cluster membership, better spectroscopic data, emphasis on gathering “complete” RG samples in individual clusters, and new laboratory transition studies combine to make OCs attractive targets for chemical composition analyses. OCs have typically less than a few thousand members and ages less than several Gyr, and so each cluster has relatively few RGs to study.

The general aim of our project is to present abundance analyses of all known non-variable RG members of about 20 OCs. Our main focus is to determine the LiCNO abun-

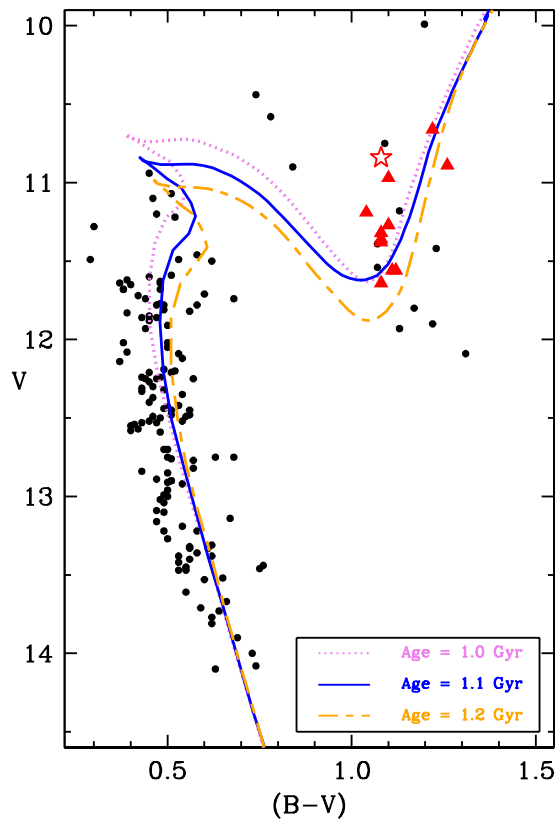


Figure 1. The observed CMD of NGC 6940 and three Yonsei-Yale isochrones. Red triangles are RGs analyzed in this study and the single red star is MMU 152 (to be discussed later). We also show isochrones for three different ages. These isochrones have been shifted to match the observed CMD by applying the reddening and distance modulus of NGC 6940 given in Table 1.

dances and $^{12}\text{C}/^{13}\text{C}$ ratios, and to try to evaluate the evolutionary status of RG members of the OCs. We are beginning with detailed studies of a couple of OCs with relatively large numbers of RGs. In the first paper of this series, (Böcek Topcu et al. 2015, hereafter Paper I) we analyzed high-resolution spectra of 10 RG members of NGC 752. We confirmed memberships of RGs by measuring radial velocities (RV), determined model atmospheric parameters, and derived detailed chemical compositions. We also were able to estimate the evolutionary status of individual RGs by using their photometric and spectroscopic CMD properties along with the light element abundances.

In this paper we report on a similar investigation of NGC 6940. Like NGC 752 of Paper I, NGC 6940 contains a relatively large population of RGs: the WEBDA³ OC database suggests that there are ~ 20 RG members of this cluster. NGC 6940 has been mostly neglected in the literature. To our knowledge this work presents the chemical composition analysis of the first large sample that includes 12 purported RG members of NGC 6940. We have gathered high resolution, high signal-to-noise spectra. We report RVs, atmospheric parameters, $[\text{Fe}/\text{H}]$ metallicities⁴, and detailed abundances of the α , light odd-Z, Fe-peak, and neutron-

³ <http://www.univie.ac.at/webda/webda.html>⁴ For elements A and B, $[\text{A}/\text{B}] = \log (N_{\text{A}}/N_{\text{B}})_{\star} - \log$ ² <http://www.astro.ufl.edu/~ata/wocs/>

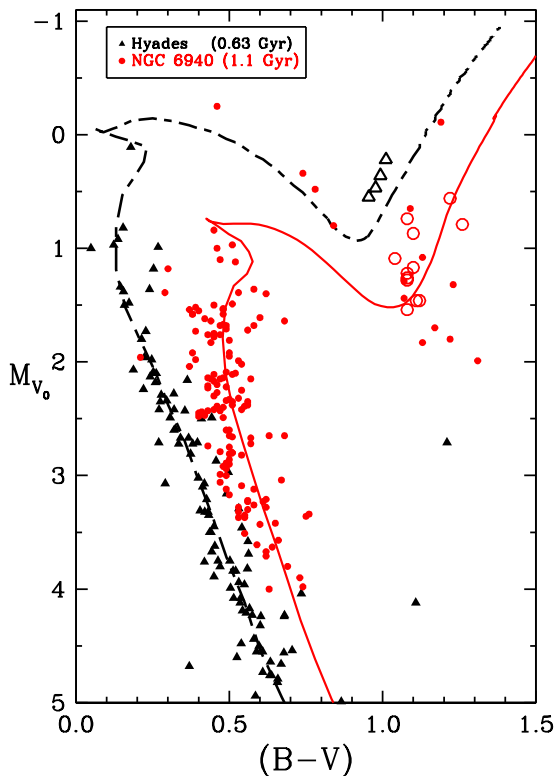


Figure 2. Color-absolute magnitude diagram of the open clusters NGC 6940 and Hyades with Yonsei-Yale isochrones. Open symbols represent the RGs analyzed in this study.

capture groups, with a particular focus on the LiCNO elements. We also include abundance analysis of the four well-known RG members of the Hyades open cluster in order to standardize our analysis of NGC 6940.

The structure of this paper is as follows: in §2 we summarize the history of NGC 6940 and its RGB members. The observations and reductions are outlined in §3. We discuss compilation of atomic/molecular line lists and equivalent width measurements in §4. The derivation of model atmospheric parameters is described in §5, followed by abundance analysis in §6. Finally, in §7 we discuss the implications of our results for the evolution of NGC 6940.

2 NGC 6940

NGC 6940 is an intermediate age (≈ 1 Gyr) open cluster at a distance of $d \approx 800$ pc; overall cluster parameters are gathered in Table 1. NGC 6940 has probably not been studied extensively because its members are not easily distinguished from field stars along the same sight line. Trumpler (1930) classified this cluster as III 1m, meaning that it is a detached cluster with no noticeable central concentration, containing 50-100 stars of nearly the same apparent magnitude. The star numbering system of NGC 6940 is mostly based on Vasilevskis & Rach (1957), as reorganized

by Mermilliod et al. (2008). We have adopted this numbering system, adding the prefix “MMU” for star names in this paper.

2.1 Previous Studies

Two early studies of OC RGs included NGC 6940. Using Walker (1958) data, Hartwick & McClure (1972) studied NGC 6940 as part of an investigation focused on $E(U - B)/E(B - V)$ color excess ratio, and found fairly uniform reddening. Assuming a commonly used color excess ratio of 0.72, they derived $E(B - V)_{ms} = 0.20 \pm 0.005$, $E(B - V)_{giants} = 0.18 \pm 0.012$. Jennens & Helfer (1975) derived metallicities, color excesses and distance moduli for 20 clusters by observing their K-giants with UBVI_z photometry. They observed 20 RGs in NGC 6940 and calculated the following quantities: $[\text{Fe}/\text{H}] = -0.2$, $E(B - V) = 0.16$, $(m - M)_0 = 10.2$ and age $t = 5 \times 10^8$ yr.

The first relative proper motion study of NGC 6940 to estimate cluster membership was conducted by Vasilevskis & Rach (1957). The cluster drew some attention in this era because it contains a semi-regular M0 giant (FG Vul) and it appears to have a peculiar RGB with variable reddening. Because of these reasons it has been subject to many photographic and photometric studies in UB_V system such as Walker (1958), Larsson-Leander (1960), Hoag et al. (1961), and Johnson et al. (1961). Various photometric and membership studies were cross-correlated by Larsson-Leander (1964), who concluded that interstellar reddening is irregular across the cluster face ($E(B - V) = 0.05$ to 0.30 , Tagliaferri & Belloni (1997).)

Geisler (1988) has conducted one of the first extensive radial velocity (RV) study of NGC 6940. Geisler derived the mean cluster RV, $\langle \text{RV} \rangle = 5.7 \pm 1.5$ km s⁻¹, by gathering medium-resolution spectroscopy of 11 stars. Mermilliod & Mayor (1989) conducted the RV study of NGC 6940, using observations of 24 possible member RGs. Rejecting four of the targets as non-members, they derived a mean cluster velocity of $\langle \text{RV} \rangle = 7.75 \pm 0.13$ km s⁻¹ from the 20 RG members, and found that six of them are spectroscopic binaries. Recently, Mermilliod et al. (2008) observed 26 possible NGC 6940 RGs, finding five of them to be non-RV members. They also updated their previous RV measurements and derived a cluster velocity of $\langle \text{RV} \rangle = 7.89 \pm 0.14$ km s⁻¹. Additionally, they discussed the morphology of the cluster RGB in general, noting in particular star MMU 152, one of our chosen targets. This RG appears to have the CMD location of a typical binary RG, but it did not show any variability in its velocity data. Therefore, they concluded that MMU 152 is possibly a double star with large separation.

Strobel (1991b) calculated “absolute” metallicities of 72 OCs from previous spectroscopic and photometric studies, obtaining $[\text{M}/\text{H}] = -0.1$ for NGC 6940 with probable error not larger than 0.1 dex. In a companion paper, Strobel (1991a) suggested that $[\text{M}/\text{H}] = -0.14$ from consideration of the age and Galactic position of NGC 6940. The mean of more recent metallicity estimates generally agree on a solar metallicity for this cluster, albeit with some scatter. Thøgersen et al. (1993) obtained moderate-resolution CCD spectra and measured $[\text{Fe}/\text{H}]$ values via Mg and Fe spectroscopic indices, finding $[\text{Fe}/\text{H}] = -0.06 \pm$

$(N_A/N_B)_\odot$ and $\log \epsilon(A) = \log (N_A/N_H) + 12.0$. Also, metallicity will be taken to be the $[\text{Fe}/\text{H}]$ value.

Table 2. Basic parameters of observed NGC 6940 RGs.

Star	RA (2000)	DEC (2000)	B^a	V^a	K^b	M_{V_0}	$(B - V)$	$(B - V)_0$	$(V - K)_0$	μ_α (mas/yr)	μ_δ (mas/yr)
MMU 28 ^c	20 33 25.016	+28 00 46.97	12.68	11.56	8.93	1.46	1.12	0.91	2.42	-5.70	-14.6
MMU 30 ^c	20 33 29.806	+28 17 05.07	12.15	10.89	8.18	0.79	1.26	1.05	2.50	-5.70	-7.6
MMU 60 ^d	20 33 59.570	+28 03 01.64	12.67	11.56	8.97	1.46	1.11	0.90	2.38	-3.4	-8.1
MMU 69 ^d	20 34 05.746	+28 11 18.38	12.72	11.64	8.95	1.54	1.08	0.87	2.48	+1.5	-9.6
MMU 87 ^d	20 34 14.693	+28 22 15.76	12.40	11.32	8.74	1.22	1.08	0.87	2.37	-3.3	-11.0
MMU 101 ^d	20 34 23.645	+28 24 25.62	12.37	11.27	8.74	1.17	1.10	0.89	2.32	-2.6	-8.7
MMU 105 ^c	20 34 25.458	+28 05 05.62	11.88	10.66	7.82	0.56	1.22	1.01	2.63	-5.0	-13.0
MMU 108 ^c	20 34 25.675	+28 13 41.54	12.23	11.19	8.70	1.09	1.04	0.83	2.28	-3.4	-11.4
MMU 132 ^c	20 34 40.112	+28 26 38.94	12.07	10.97	8.40	0.87	1.10	0.89	2.37	-6.8	-17.6
MMU 138 ^d	20 34 45.875	+28 09 04.62	12.44	11.36	8.81	1.26	1.08	0.87	2.34	-4.8	-12.8
MMU 139 ^d	20 34 47.610	+28 14 47.25	12.46	11.38	8.80	1.28	1.08	0.87	2.37	+0.1	-7.5
MMU 152 ^{c,d}	20 34 56.637	+28 14 27.27	11.92	10.84	8.27	0.74	1.08	0.87	2.36	-1.9	-4.6

^a Larsson-Leander (1960)^b Cutri et al. (2003)^c Coordinates and proper motions from Hog et al. (1998)^d Coordinates and proper motions from Høg et al. (2000)

0.13 for NGC 6940 from six RG members. The Dias et al. (2002) OC compendium⁵ recommends $[\text{Fe}/\text{H}] = +0.04 \pm 0.10$. Twarog et al. (1997) included NGC 6940 in their investigation of photometric and spectroscopic data for 76 open clusters, deriving $[\text{Fe}/\text{H}] = 0.01 \pm 0.06$. Friel et al. (2002) calculated metallicity by using the spectroscopic data from Thøgersen et al. (1993), finding $[\text{Fe}/\text{H}] = -0.12 \pm 0.10$. By using Hoag et al. (1961) photometric data Cameron (1985) calculated $[\text{Fe}/\text{H}] = 0.014$ from transformed ultraviolet excesses. Recently, Blanco-Cuaresma et al. (2015) included one NGC 6940 RG in their high-resolution “chemical tagging” spectroscopic study of 31 OCs. Abundances of 17 species and $[\text{Fe}/\text{H}]$ was derived for this one RG member of NGC 6940 from the NARVAL spectropolarimeter ($R \cong 81,000$) data. They calculated metallicities from two slightly different normalization processes: $[\text{Fe}/\text{H}]_1 = +0.04$ and $[\text{Fe}/\text{H}]_2 = +0.09 \pm 0.07$. From all of these studies we conclude that NGC 6940 has near-solar overall metallicity.

2.2 Colour-Magnitude diagram and RG target selection

Photometric and photographic observations of NGC 6940 have been done by several authors (e.g. Walker 1958; Larsson-Leander 1960; Hoag et al. 1961; Johnson et al. 1961; Larsson-Leander 1964; Stetson 2000). To our knowledge, there is no recent homogeneous photometric survey that could create a comprehensive CMD that includes our target RGs. Therefore we chose to use photographic colors and magnitudes compiled from the sources provided in WEBDA database. In Figure 1 we have plotted the data from Larsson-Leander (1960). These data contain 164 probable members of NGC 6940. Sanders (1972) reported astrometric cluster membership probabilities of 216 stars in the field of the NGC 6940. 115 stars in Larsson-Leander (1960) list are confirmed as members of this cluster by Sanders

(1972). The rest of the Larsson-Leander sample are not included in Sanders’s study. All our RGs are confirmed as the members of the NGC 6940 open cluster in Sanders (1972); Mermilliod & Mayor (1989) and Mermilliod et al. (2008). Also 10 of the RGs we studied here have been presented in the catalog of membership probabilities published by Dias et al. (2014) and they all have membership probabilities over 90%. In Figure 1 we also show three isochrones from the latest set of the Yonsei-Yale (Y^2) project (Demarque et al. 2004)⁶. To match the observations we applied the reddening and distance modulus values given in Table 1, and have assumed $A_v = 3.1E(B - V)$. Our main goal was to estimate the turn-off mass for the cluster and use this information to have a better estimate on the model atmospheric parameters of the cluster members (see §5.1). The best average match between the NGC 6940 observed CMD and Y^2 isochrones is for an age $\log(t) = 9.04$ (1.1 Gyr), somewhat older than the WEBDA value of 8.86, and for a metallicity $Z = 0.016$ (equivalent to $[\text{M}/\text{H}] = -0.06$). We also tried matching other sets of isochrones to the data besides Y^2 , such as PARSEC (Bressan et al. 2012) and Dartmouth (Dotter et al. 2008), finding that Y^2 isochrones provide the best-fitting model isochrone to the cluster data. However, the different isochrone grids all yielded similar results, suggesting a turn-off mass range from 1.9 to 2.1 M_\odot for NGC 6940. Therefore we have decided to adopt an average turn-off mass of $M_{\text{TO}} = 2 M_\odot$ for this cluster.

The WEBDA age of NGC 6940 listed in Table 1, $\log(t) = 8.86$ was adopted from Loktin et al. (2001). Lynga (1995)⁷ recommended $\log(t) = 9.04$, taking their value from van den Bergh & McClure (1980). Kharchenko et al. (2005) reports $\log(t) = 8.94$ for the cluster. We also applied Y^2 isochrones to the well-known open cluster Hyades to compare the two clusters, thus gaining more confidence in the age estimate of NGC 6940. The Hyades age is very well

⁵ <https://heasarc.gsfc.nasa.gov/W3Browse/all/openclust.html>⁶ <http://www.astro.yale.edu/demarque/yyiso.html>⁷ <http://cdsarc.u-strasbg.fr/cgi-bin/mvcat3?VII/92A>

determined, $\log(t) = 8.80$ (625 ± 25 Myr, Perryman et al. 1998), as is its main sequence turn-off mass, $2.3 M_{\odot}$ (Weidemann et al. 1992). Using the photometric data of Hyades taken from Johnson & Knuckles (1955), we compare the isochrone fittings of both clusters in Figure 2. As in Figure 1 we added extinction to the (B-V) isochrones in Figure 2, to separate clearly the NGC 6940 and Hyades OC sequences. We have transformed V into M_{V_0} using the parameters of Table 1, again assuming $A_v = 3.1E(B - V)$. It is clear that NGC 6940 is much older than Hyades, and we accept the age implied by our Y^2 isochrone fit, $\log(t) = 9.04$.

Further refinement of cluster membership was accomplished in the RV survey of Mermilliod et al. (2008), who observed 26 RG possible member of NGC 6940 with CORAVEL “spectrovelocimeter”. They derived $\langle RV \rangle = 7.89 \pm 0.14$ for NGC 6940, and used that mean velocity to eliminate five probable non-members, paring the list to 21 RGs. Our target list contains 13 stars from that study, after the elimination of an additional eight stars suggested to be spectroscopic binaries or have variable velocities in the Mermilliod et al. survey. We were able to gather high resolution spectra of 12 of these member RGs. Program stars are listed in Table 2 by their MMU designations, along with their coordinates and proper motions from SIMBAD⁸, B and V magnitudes from Larsson-Leander (1960), and K magnitudes from 2MASS (Cutri et al. 2003). Table 2 also contains observed $(B - V)$ color indexes, de-reddened $(B - V_0)$ and $(V - K_0)$ values, and absolute magnitudes M_{V_0} . Our NGC 6940 RGs are marked with red triangles and star in Figure 1. These occupy a very small CMD domain: $0.85 \leq B - V \leq 1.05$, $0.5 \leq M_V \leq 1$.

3 OBSERVATIONS AND REDUCTIONS

High-resolution ($R \equiv \lambda/\Delta\lambda \approx 60,000$) spectra of target RGs were gathered with the McDonald Observatory 9.2m Hobby-Eberly Telescope (HET) High-Resolution Spectrograph (HRS; Tull 1998). This instrument achieves a large spectral coverage from a mosaic of two CCD detectors. In the configuration adopted for this project the spectral coverage is 5100–6900 Å on the “blue” detector and 7000–8800 Å on the “red” detector. Observations were conducted between April and June of 2013. Individual exposure times and S/N ratios are given in Table 3. Two exposures were taken for each target. Our stars are solar-metallicity RGs and thus have very line-rich spectra. Therefore it is very difficult to find pure continuum regions to specify S/N ratios from the reduced spectra. The S/N ratios in Table 3 are taken from the observing night reports of the HET.

After splitting the raw data images into red and blue sections, we applied standard reduction procedures for both sections by using IRAF⁹ routines. We started with over-scan removal, bias subtraction, flat-fielding and scattered light subtraction with the tasks in the *ccdred* package. Then commands of the *echelle* package were used to extract the single-order spectra. We used the *ecidentify* task for wavelength calibration, based on ThAr lamp exposures taken

each observing night. Removal of the telluric (atmospheric) lines was conducted with *telluric* task, which divides out the telluric lines from the spectrum of the program star by using the spectrum of a hot, rapidly rotating (telluric) star obtained in the same observing night.

High resolution ($R \approx 60,000$) observations of four RGs of the Hyades open cluster were conducted with the Robert G. Tull Cross-Dispersed Echelle Spectrograph (Tull et al. 1995) on the 2.7 m Harlan J. Smith Telescope at McDonald Observatory in October 2012. The spectral coverage of this setup is 4000–8000 Å and we applied the same reduction procedure as described above.

To measure the RVs of the OC members we used synthetic spectra that we created using the same line list (described in §4) as templates. These templates have similar T_{eff} , $\log g$, and $[\text{Fe}/\text{H}]$ to our program stars. We determined four clear spectral orders that have as many stellar lines as possible without much telluric contamination both in blue and red regions, and then created template synthetic spectra for the wavelength regions of 8290–8430 Å, 7960–8090 Å, 7390–7505 Å, 7030–7160 Å in the red, and 6720–6840 Å, 5990–6090 Å, 5710–5800 Å 5260–5350 Å in the blue. Heliocentric corrections were made with the *rvcorrect* task in IRAF. Then the RV values were calculated for each region using the cross-correlation task *fxcor* (Fitzpatrick 1993). In Table 3, we list the final RV values along with their standard deviations (σ) for each star, which we achieved by taking the average of RVs measured from individual regions.

The difference between the average of *fxcor* errors and standard deviations of eight RVs vary from star to star in the range 0.05–0.10 km s⁻¹. The mean RV of the cluster, $\langle RV \rangle = 8.02 \pm 0.16$ km s⁻¹ ($\sigma = 0.56$), agrees with the Mermilliod et al. (2008) value ($\langle RV \rangle = 7.89 \pm 0.14$ km s⁻¹) within mutual uncertainties.

Table 3 also contains RVs of each star reported by Mermilliod et al. (2008). According to our RV determinations MMU 28 deviates from the cluster mean by $+0.88$ km s⁻¹ ($\sigma = 1.5$ km s⁻¹) and MMU 152 by $+1.26$ km s⁻¹. These RVs may lower their stars’ cluster membership probabilities slightly but membership in NGC 6940 is not ruled out. The proper motion membership probabilities given for MMU 28 and MMU 152 by Sanders (1972) are 60 and 94%, respectively. Dias et al. (2002) report only the proper motion membership probability for MMU 152 and it is also over 90%. RV membership probabilities were discussed by Mermilliod & Mayor (1989) and Mermilliod et al. (2008), they both confirmed the membership status of both stars.

If we combine our values with those of Mermilliod et al. (2008) we conclude that all the RGs we have observed are members of NGC 6940 with high probabilities.

4 LINE LISTS AND EQUIVALENT WIDTHS

To evaluate the atmospheric parameters and chemical abundances of all species we used the current version of the LTE line analysis and synthetic spectrum code MOOG¹⁰ (Sneden 1973). Two techniques were employed to derive the

⁸ <http://simbad.u-strasbg.fr/simbad/>

⁹ <http://iraf.noao.edu/>

¹⁰ <http://www.as.utexas.edu/~chris/moog.html>

Table 3. Exposure times and radial velocities of the observed stars.

Star	Exp. (s)	S/N @6948 Å	RV^a (km s ⁻¹)	σ	RV^b (km s ⁻¹)
MMU 28	1000	130	8.90±0.08	0.22	7.99±0.16
MMU 30	700	113	7.96±0.07	0.20	7.63±0.15
MMU 60	1050	121	7.66±0.08	0.22	7.27±0.18
MMU 69	1050	93	8.08±0.08	0.24	7.56±0.15
MMU 87	900	103	7.98±0.09	0.27	7.45±0.16
MMU 101	900	155	7.74±0.08	0.23	6.81±0.14
MMU 105	650	116	7.74±0.08	0.23	7.58±0.13
MMU 108	900	145	7.39±0.09	0.25	6.76±0.13
MMU 132	700	129	7.76±0.15	0.42	7.17±0.14
MMU 138	900	82	8.22±0.08	0.23	7.55±0.15
MMU 139	900	136	7.53±0.08	0.23	7.12±0.16
MMU 152	650	144	9.28±0.08	0.24	8.50±0.15

^a this study^b Mermilliod et al. (2008)

chemical abundances: equivalent width (EW) measurement and spectral synthesis. Measured EW s of unblended neutral and ionized Fe and Ti were used to calculate the atmospheric parameters. Abundances from Si I, Ca I, Cr I, Cr II and Ni I transitions were also derived from EW measurements. The other atomic and molecular species, which have spectral lines that are blended and/or afflicted by hyperfine/isotopic substructure, were analyzed using the spectral synthesis technique.

4.1 Line Lists

In Paper 1 on OC NGC 752 we generated a line list of relatively unblended lines that have reliable transition probabilities in the yellow-red spectral region. For the present study we used a slightly updated line list with some addition of Fe I and Ni I lines. The complete line list, which includes both these EW transitions and those later to be used in spectrum syntheses, is presented in the online version of the Table 4, which contains wavelengths λ , lower excitation energies χ , transition probabilities $\log gf$, and references for the transition probabilities.

The chosen wavelength range of EW measurements was 5200–7100 Å. We tried to avoid regions of heavy telluric line contamination, and did not explore the crowded bluer spectral regions ($\lambda < 5100$ Å) since the determination of their continua is difficult.

We derived the model atmospheric parameters from 71 Fe I, 12 Fe II, 11 Ti I and 4 Ti II lines; the numbers vary from star to star. After several trials we put some restrictions to the Fe and Ti transitions that were used to calculate the model atmosphere parameters. In particular, we discarded very weak and strong lines for these species by limiting the EW s to $10 \text{ mÅ} < EW < 150 \text{ mÅ}$, or $RW = \log(EW/\lambda) \sim -5.8$ to -4.6 at $\lambda \simeq 6400$ Å. We did not apply the EW limitation to other species.

We have adopted various references for the transition probabilities. When possible we tried to use laboratory-based homogeneous (single source) gf and isotopic/hyperfine structure data. Unfortunately, there are no

Table 4. Atomic transitions used in this study. The machine-readable version of the entire table is available in the online journal.

Species	Wave. (Å)	LEP (eV)	$\log gf$	EW / syn	Ref.
Li I	6707.9	0	0.17	syn	Kurucz
CH	4310			syn	Mas14 ^a
CH	4325			syn	Mas14
C ₂	5160			syn	Bro14 ^b
C ₂	5630			syn	Bro14
CN	8000			syn	Sne14 ^c
O I	6300.31	0	-9.72	syn	Allen01 ^d
Na I	5682.64	2.101	-0.71	syn	NIST
Na I	6154.23	2.101	-1.55	syn	NIST
Na I	6160.75	2.103	-1.25	syn	NIST
Mg I	5528.41	4.343	-0.62	syn	Kurucz
Mg I	5711.08	4.343	-1.83	syn	Kurucz
Mg I	7811.11	5.941	-0.95	syn	Kurucz
Al I	6696.02	3.14	-1.35	syn	Kurucz
Al I	6696.18	4.018	-1.58	syn	Kurucz
Al I	6698.67	3.14	-1.64	syn	Kurucz
Al I	7835.30	4.018	-0.65	syn	Kurucz
Si I	5488.98	5.614	-1.90	EW	Lob11 ^e
Si I	5517.53	5.082	-2.61	EW	VALD
Si I	5665.55	4.92	-2.04	EW	NIST

^a Masseron et al. (2014)^b Brooke et al. (2014)^c Sneden et al. (2014)^d Allende Prieto et al. (2001)^e Lobel (2011)

recent comprehensive lab studies for the important species Fe I and Fe II, so for them we had to use several sources (e.g. O'Brian et al. 1991, Den Hartog et al. 2014, Ruffoni et al. 2014, NIST¹¹, and VALD¹² (eg. Ryabchikova et al. 2015)). The useful spectral range of the HET data for our OC work is a little different from that of the McDonald 2.7m data, so we added twenty more Fe I lines to the list used in Paper 1. Most of the new lines are from Den Hartog et al. and Ruffoni et al.. For the species Ti I, Ti II, V I, Cr I, Co I, Ni I, La II, Nd II and Eu II we exclusively used lab data obtained by the University of Wisconsin atomic physics group.

For the present study, we investigated some of the potentially blended lines more closely and updated the gfs of a few lines as well as the number of lines used for the abundance determinations for some species. All of these changes were first tested on the very high-resolution solar (Kurucz et al. 1984) and Arcturus flux spectra (Hinkle et al. 2000). Line lists for a few individual species deserve comment here.

Manganese: As in Paper 1, we determined manganese abundances from the Mn I the triplet around 6016 Å region. We used synthetic spectra due to the many hyperfine structure (hfs) components that make up each of these transitions. Investigation of the 6016.7 Å Mn I line profile using both solar and Arcturus spectra showed that a Fe I line at

¹¹ http://physics.nist.gov/PhysRefData/ASD/lines_form.html¹² <http://vald.inasan.ru/~vald3/php/vald.php>

Table 5. Equivalent width measurements (mÅ) of the first five lines for the RGs of the NGC 6940. The machine-readable version of the entire table is available in the online journal.

Species	Wavelength (Å)	MMU											
		28	30	60	69	87	101	105	108	132	138	139	152
Si I	5488.98	31.3		32.1	31.6		31.7		28.2	40.0		35.1	
Si I	5517.53	22.5	29.6	25.5	27.6				21.2	30.1	25.7	24.3	29.4
Si I	5665.55	64.4	71.9		63.4		66.0		61.7	73.4	62.5	67.6	
Si I	5690.43	61.9	69.1	61.0	62.7	72.5	65.4		62.3		63.5		
Si I	5772.15	68.3					75.2		65.6	80.2		71.3	77.3

6016.61 Å is blended with the Mn *hfs* and creates an unrealistic asymmetric line profile around the Mn I components, which in turn affects the Mn abundance determined from this line. Proper accounting of the Fe I blend allowed us to measure internally consistent Mn abundances from the triplet around 6016 Å.

Copper: In this study, we used only the 5782.13 Å Cu I transition, adopting the overall *gf* value and the isotopic and hyperfine splitting from Cunha et al. (2002), who used the laboratory data of Hannaford & Lowe (1983). We assumed solar-system isotopic percentages of ⁶³Cu (69.2%) and ⁶⁵Cu (30.8%). We were not able to use other Cu I lines located at 5218.2 and 5220.06 Å due to severe atomic and molecular line contamination. The prominent 5105.5 Å line lies outside our HET HRS spectrum coverage.

Yttrium and Neodymium: We used only Y II lines for this element. We added four more lines to the list used in Paper I, but we had to drop 5087.42 Å from the present study; it is also beyond the HRS coverage. We also added two more lines in the analysis of Nd II.

Scandium, Vanadium, and Cobalt: In Paper I, we had to give special treatment to the Fe-group species of V I, Co I and Sc II transitions since they have significant hyperfine substructure and lacked recent lab studies. Their abundances were computed from *EWs* input to MOOG’s blended-line option *blends* after deriving empirical transition probabilities from the solar spectrum. For the present work, we were able to adopt new V I laboratory data from Lawler et al. (2014), and new lab Co I data from Lawler et al. (2015). These fresh line data include improved hyperfine substructure parameters. No lab studies for Sc II have been published recently, so we used reverse solar to calculate their line transition probabilities. That is, we measured *EWs* from a very high-resolution solar flux spectrum (Kurucz et al. 1984) and forced their *gfs* to give the solar abundances recommended by Asplund et al. (2009). We then used these calculated *gfs* in similar calculations for the program stars.

Since later in the paper we compare the abundances of NGC 6940 and Hyades clusters with NGC 752 results, we applied these new updates to the fresh analyses of NGC 752 RG stars. We will discuss these new values (Table 12) in §7. The remaining species (C₂, CN, [O I], Li I, Na I, Mg I, Cu I, Zn I, Y II, La II, Nd II, Eu II) have complex transition substructures and/or are blended with various atomic and/or molecular lines. We derived their abundances by spectrum synthesis with the MOOG *synth* option.

4.2 Equivalent width measurements

We used the same Interactive Data Language (IDL) code (Roederer et al. 2010; Brugamyer et al. 2011) to measure the *EWs* that was described in Paper I. This interactive code automatically matches the observed lines with theoretical Gaussian line profiles or Voigt profiles for some of the stronger lines. Line depths were also recorded to estimate the initial effective temperatures T_{eff} (§5) using the line depth ratio (LDR) method, to be described in §5.1. We present *EW* measurements of our 12 NGC 6940 RGs in Table 5.

5 MODEL ATMOSPHERES

We made use of the *EWs* of unblended neutral and ionized Fe and Ti lines to determine the model atmospheric parameters (T_{eff} , $\log g$, ξ_t , [M/H]) of our program stars. Fe and Ti abundances were processed simultaneously with the semi-automated version of MOOG. Each atmospheric parameter is connected to the abundances of these species as follows: (i) for T_{eff} , abundances of low- and high-excitation potential (χ) lines of Fe I and Ti I need to be the same on average; (ii) for ξ_t , there should be no apparent trend between the reduced width ($RW = \log(EW/\lambda)$) and abundances of neutral weak and strong lines of Fe I and Ti I; (iii) for $\log g$, mean abundances of neutral and ionized Fe and Ti lines need to be in agreement; (iv) and for [M/H], derived metallicity should agree with the one assumed in creating the model atmosphere.

In estimating model parameters we applied the same weights to Fe and Ti species that were described in Paper I. That is, we gave 0.65 weight to Fe lines, and 0.35 for Ti lines. MOOG first calculated the abundances from the individual line *EWs* with an initial model atmosphere. Then it iteratively altered the input model parameters in response to the abundance slopes with χ and RW , until a balance was achieved between the neutral and ionized species for a final model atmosphere.

5.1 Initial parameters

To determine the initial model atmosphere parameters, we applied the same methods and equations as described in Paper I. A detailed description is given in that paper; a brief summary is given here. Photometric effective temperatures were calculated from $(B-V)_0$, and $(V-K)_0$ colors (Table 2) using the metallicity-dependent T_{eff} -color calibrations given by Ramírez & Meléndez (2005) for giant stars. We also derived LDR temperatures directly from the spectra. The LDR

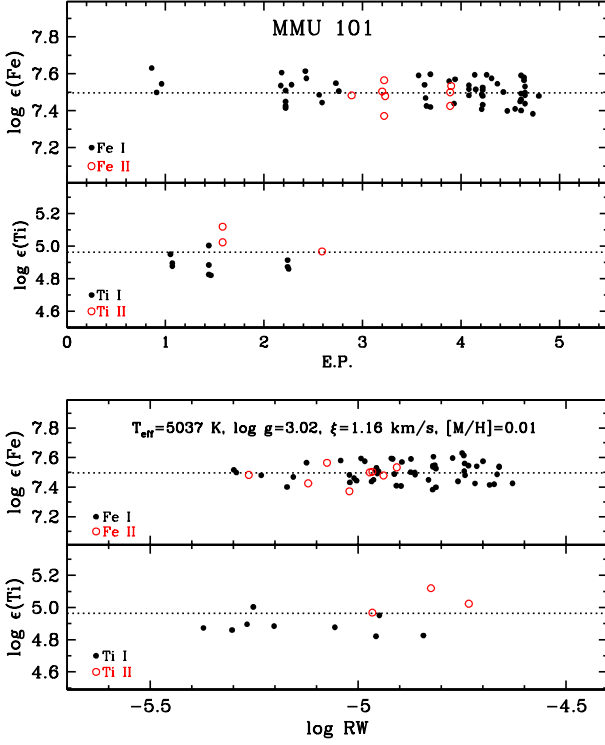


Figure 3. An example model atmosphere parameter determination using both ionized and neutral species of Fe and Ti for MMU 101. In the top panel the line abundances are plotted as a function of excitation potential χ (E.P.), and in the bottom panel as a function of reduced width RW. Iterating $T_{\text{eff,spec}}$, $\log g$, and ξ_t until there was no significant dependence of abundances with E.P. and RW, and until agreement was attained between abundances derived from neutral and ionized species, led to the final model parameter choices given in the bottom panel.

method was developed by Gray & Johanson (1991) and refined by several authors (Strassmeier & Schordan 2000; Gray & Brown 2001; Biazzo et al. 2007a,b, e.g.). We measured the line depths of many lines in the 6190–6280 Å spectral region, and formed LDR’s for 12 line pairs out of the 22 that were recommended by Biazzo et al. (2007a). Using her polynomial coefficients for non-rotationally broadened stars we estimated the individual $T_{\text{eff,LDR}}$ from these LDR’s. Calculated $(B - V)_0$, $(V - K)_0$ ¹³ and LDR temperatures with their standard deviations are listed in Table 6. Since $(V - K)_0$ colors are nearly independent of metallicity, for the stars that have K magnitudes we used non-weighted averages of $T_{\text{eff,(V-K)}}$ and $T_{\text{eff,LDR}}$ as initial T_{eff} estimates.

We used the following standard equation to compute the initial physical gravities of the cluster members.

$$\log g_{phy} = 0.4 (M_{V\star} + BC - M_{\text{Bol}\odot}) + \log g_{\odot} + 4 \log \left(\frac{T_{\text{eff}\star}}{T_{\text{eff}\odot}} \right) + \log \left(\frac{m_{\star}}{m_{\odot}} \right). \quad (1)$$

Solar parameters adopted in this equation are: M_{bol} =

¹³ The K magnitude is from 2MASS, and Ramírez & Meléndez (2005) label the color $(V - K_2)$.

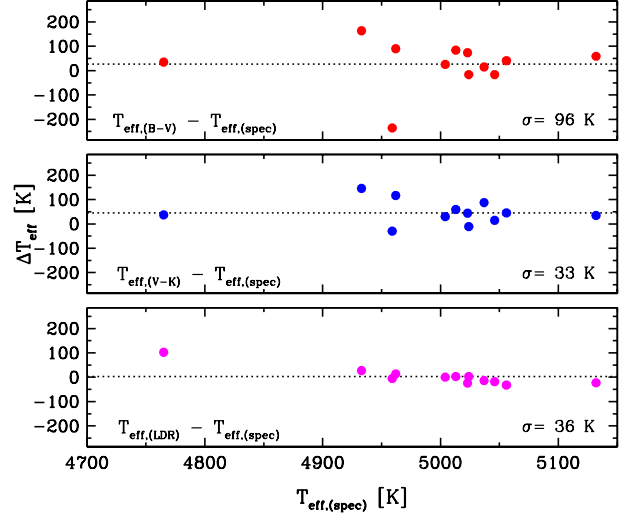


Figure 4. Differences between initial T_{eff} estimates and derived spectroscopic temperatures $T_{\text{eff(spec)}}$ plotted as a function of the $T_{\text{eff,spec}}$ values. Dotted lines in the panels indicate the mean differences and the standard deviations of the differences are given in each panel. The top panel contains photometric $T_{\text{eff,(B-V)}}$ values, the middle panel has photometric $T_{\text{eff,(V-K)}}$ values, and the bottom panel has spectroscopic $T_{\text{eff,LDR}}$ values.

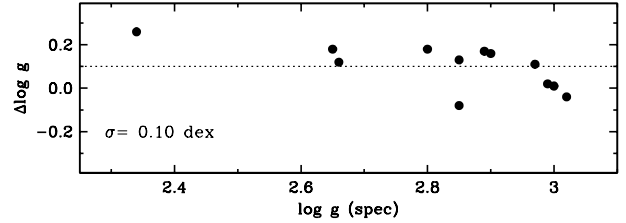


Figure 5. Differences between the physical gravities $\log g_{phy}$ computed with Eq. 1 and the spectroscopic gravities $\log g_{spec}$ derived from ionization balances of Fe and Ti, plotted as a function of $\log g_{spec}$. A dotted line indicates the mean difference.

4.75, $\log g = 4.44$, and $T_{\text{eff}} = 5777$ K. The polynomial formula and coefficients given in Table 1 of Torres (2010) were used to calculate the temperature-dependent bolometric corrections. Absolute magnitudes of the target RGs were derived by using the cluster distance modulus and reddening (Table 1). For the masses of the RGs we used a turn-off mass of $2 M_{\odot}$ (see §2.2). With the guidance of previous studies (§2.1), we adopted initial metallicities of $[M/H] = 0.0$ and microturbulent velocities of $\xi = 1.20 \text{ km s}^{-1}$.

5.2 Final parameters

To obtain the final model atmosphere parameters, we used the EW s of neutral and ionized Fe and Ti lines, initial model atmosphere parameters, cluster distance modules and reddening along with the magnitudes of RGs as inputs in the semi-automated model iteration code. Stellar atmosphere models with opacity distribution functions and no convective overshooting were calculated using the grids of ATLAS9 Model Atmospheres from Castelli & Kurucz (2003). Software developed by Andy McWilliam and Inese Ivans that interpolates the grids to achieve the final model atmosphere

Table 6. Photometric and spectroscopic atmospheric parameters.

Star	$T_{\text{eff},(B-V)}$ (K)	$T_{\text{eff},(V-K)}$ (K)	$T_{\text{eff},(LDR)}$ (K)	$\log g_{\text{phy}}$ (cm s^{-2})	$T_{\text{eff},\text{spec}}$ (K)	$\log g_{\text{spec}}$ (cm s^{-2})	ξ_{spec} (km s^{-1})	[M/H]
NGC 6940								
MMU 28	5008	5013	5027 ± 33	3.06	5024	2.89	1.03	−0.05
MMU 30	4724	4929	4954 ± 39	2.77	4959	2.85	1.32	−0.06
MMU 60	5030	5061	5028 ± 19	3.08	5046	2.97	0.97	−0.02
MMU 69	5030	5034	5004 ± 29	3.06	5004	2.90	1.05	−0.03
MMU 87	5097	5067	4999 ± 43	2.98	5023	2.85	1.07	0.03
MMU 101	5052	5125	5023 ± 22	2.98	5037	3.02	1.16	0.01
MMU 105	4800	4802	4867 ± 36	2.60	4765	2.34	1.35	−0.15
MMU 108	5191	5167	5109 ± 17	2.98	5132	2.8	1.28	−0.16
MMU 132	5052	5079	4976 ± 37	2.83	4962	2.65	1.29	−0.12
MMU 138	5097	5101	5024 ± 30	3.01	5056	3.00	1.10	0.00
MMU 139	5097	5072	5016 ± 28	3.01	5013	2.99	1.10	0.01
MMU 152	5097	5079	4960 ± 12	2.78	4933	2.66	1.36	−0.16
Hyades								
δ Tau	4872	4918	4962 ± 33	2.65	4878	2.57	1.34	−0.03
ϵ Tau	4812	4868	4921 ± 30	2.53	4870	2.67	1.46	−0.01
γ Tau	4852	4928	4942 ± 32	2.60	4945	2.78	1.42	−0.03
θ Tau	4956	4980	4941 ± 43	2.69	4961	3.00	1.28	0.01

parameters was used as a part of the model iterations. In Figure 3 we plot final line-by-line abundance results for the star MMU 101, chosen to illustrate the final outcome of our model iteration procedure. As seen in the figure, abundances of Fe I, Fe II, Ti I and Ti II show no obvious trends with χ and RW values and also no abundance differences between the neutral and ionized species are observed. We list the initial and final model atmosphere parameters for our NGC 6940 and Hyades program stars in Table 6.

Figure 4 shows comparisons of initial photometric and LDR effective temperatures with the final spectroscopic temperatures $T_{\text{eff},\text{spec}}$. Inspection of this figure indicates agreement among these four T_{eff} estimates. Taking into account the data from all three figure panels, the average of the difference between initial photometric and LDR temperatures and final spectroscopic T_{eff} 's is $\langle T_{\text{eff},\text{initial}} - T_{\text{eff},\text{spec}} \rangle = 26$ K. Both photometric temperatures $T_{\text{eff},(B-V)}$ and $T_{\text{eff},(V-K)}$ suffer from uncertainties that arise from reddening and distance parameters. For two of the RGs the $T_{\text{eff},(B-V)}$ values deviate significantly from $T_{\text{eff},\text{spec}}$ by -235 and $+164$ K. They create the apparent large scatter in the top panel of Figure 4. Even so, the mean of the differences is just $\langle T_{\text{eff},(B-V)} - T_{\text{eff},\text{spec}} \rangle = 27 \pm 28$. $T_{\text{eff},(V-K)}$ color temperatures correlate well with spectroscopic ones, $\langle T_{\text{eff},(V-K)} - T_{\text{eff},\text{spec}} \rangle = 48 \pm 12$. All photometric and LDR temperatures are in good agreement with the $T_{\text{eff},\text{spec}}$ except for MMU 105, with $\langle T_{\text{eff},\text{LDR}} - T_{\text{eff},\text{spec}} \rangle = 2.8 \pm 10$ K. A similar exercise for the Hyades also yields good agreement among the temperature estimates, with the mean offset being -1 K ($\sigma = 36$ K).

In Figure 5 we show the differences between the calculated physical gravities (initial) and spectroscopic gravities (final). The initial and final gravities agree well within the uncertainties introduced by other parameters in Eq. 1. Defining $\Delta \log g = \log g_{\text{phy}} - \log g_{\text{spec}}$ we find $\langle \Delta \log g \rangle = 0.10$ ($\sigma = 0.10$). For the Hyades the agreement is also good, with the mean offset being -0.14 ($\sigma = 0.16$).

Since the individual standard deviations of the metallicities are about 0.06 dex, the differences in metallicities of the

members stay within the uncertainty limits and do not rule out the membership status of the RGs. The mean metallicity calculated from both Fe and Ti lines for NGC 6940 from 12 RGs is $\langle [M/H] \rangle = -0.06 \pm 0.07$.

5.3 Parameter uncertainties

We followed a very similar technique as described in Paper 1 to estimate the internal uncertainties for the atmospheric parameters. First we selected three RGs, MMU 28, MMU 101 and MMU 105, as the representatives for our sample and then applied series of analyses to their spectra to estimate the probable uncertainties in effective temperature, microturbulence velocity and gravity.

Taking each star in turn, for T_{eff} we changed the temperature by 50 K in each step (while keeping the other parameters fixed) until the average difference in abundances between low and high excitation potential Fe I lines exceeded the line-to-line scatter σ of the abundances in the final derived model atmosphere. The average uncertainty for T_{eff} computed in this manner was ~ 100 K. We did similar calculation for the microturbulence, changing ξ_t in steps of 0.1 km s^{-1} and seeing the abundance effects on neutral and ionized species of Fe and Ti, led to a ξ_t uncertainty in ξ_t of $\sim 0.2 \text{ km s}^{-1}$. Finally, changing the surface gravity in steps of 0.05 dex and computing abundance differences between neutral and ionized species of these two elements led to a log g uncertainty of ~ 0.20 dex. Unfortunately we could not investigate the external uncertainties for our sample since this is first detailed spectroscopic study of the NGC 6940 RGs in the literature.

The standard deviation (~ 0.1 dex) of the differences between the physical and spectroscopic $\log g$ values are shown in Figure 5. Since the given σ is smaller than what was found from the internal uncertainty determinations, we did not include it to our overall uncertainties. The effect of the uncertainties on the elemental abundances is given in Table 7. We only summarize the results from the analysis

Table 7. Sensitivity (σ) of derived abundances to the model atmosphere changes within uncertainty limits for the star MMU 101.

Species	$\Delta T_{\text{eff}}(\text{K})$ -100 / + 100	$\Delta \log g$ -0.20 / +0.20	$\Delta \xi_t(\text{kms}^{-1})$ -0.2 / +0.2
Li I	+ 0.10 / - 0.10	0.00 / - 0.05	- 0.05 / 0.00
C	+ 0.02 / - 0.05	+ 0.03 / - 0.02	+ 0.01 / 0.00
N	+ 0.10 / - 0.10	+ 0.02 / - 0.01	0.00 / 0.00
O	+ 0.05 / - 0.05	+ 0.12 / - 0.10	0.00 / 0.00
Na I	+ 0.09 / - 0.06	- 0.01 / + 0.01	- 0.02 / + 0.06
Mg I	+ 0.05 / - 0.09	- 0.02 / + 0.02	- 0.08 / + 0.05
Al I	+ 0.06 / - 0.05	0.00 / 0.00	0.00 / + 0.03
Si I	- 0.02 / + 0.01	+ 0.02 / - 0.04	- 0.04 / + 0.04
Ca I	+ 0.09 / - 0.09	- 0.03 / + 0.03	- 0.09 / + 0.09
Sc II	- 0.01 / 0.00	+ 0.07 / - 0.10	- 0.08 / + 0.07
Ti I	+ 0.13 / - 0.13	0.00 / + 0.01	- 0.04 / + 0.03
Ti II	- 0.02 / + 0.01	+ 0.07 / - 0.10	- 0.12 / + 0.11
V I	+ 0.15 / - 0.15	+ 0.01 / 0.00	- 0.02 / + 0.02
Cr I	+ 0.10 / - 0.10	- 0.01 / + 0.02	- 0.06 / + 0.06
Cr II	- 0.06 / + 0.05	+ 0.07 / - 0.11	- 0.08 / + 0.07
Mn I	+ 0.12 / - 0.10	0.00 / + 0.02	- 0.03 / + 0.07
Fe I	+ 0.06 / - 0.07	0.00 / 0.00	- 0.09 / + 0.09
Fe II	- 0.08 / + 0.07	+ 0.08 / - 0.13	- 0.07 / + 0.06
Co I	+ 0.08 / - 0.09	+ 0.03 / - 0.02	- 0.01 / + 0.01
Ni I	+ 0.04 / - 0.05	+ 0.02 / - 0.03	- 0.08 / + 0.07
Cu I	+ 0.05 / - 0.08	+ 0.05 / - 0.02	- 0.05 / + 0.07
Zn I	+ 0.05 / - 0.05	0.00 / - 0.10	0.00 / - 0.03
Y II	+ 0.05 / - 0.04	+ 0.07 / - 0.07	- 0.06 / + 0.06
La II	+ 0.02 / - 0.04	+ 0.07 / - 0.10	- 0.02 / 0.00
Nd II	+ 0.05 / - 0.05	+ 0.10 / - 0.08	- 0.07 / + 0.05
Eu II	- 0.02 / - 0.02	+ 0.06 / - 0.13	- 0.03 / 0.00
$^{12}\text{C}/^{13}\text{C}$	- 1 / + 1	0 / + 1	0 / 0

of MMU 101, which in turn represents the overall sample. Since the observed spectrum at 8000 Å used for the $^{12}\text{C}/^{13}\text{C}$ determination of MMU 101 ($^{12}\text{C}/^{13}\text{C} > 25$) is relatively low, we estimated the $^{12}\text{C}/^{13}\text{C}$ uncertainties from the spectrum of MMU 152. ^{12}CN and ^{13}CN molecular lines are not really sensitive to the changes in model atmosphere parameters as it is seen also in Table 7.

6 DERIVED ABUNDANCES

As discussed in §4 we derived elemental abundances of elements from *EW* measurements and from synthetic spectrum calculations for lines that are blended or have hyperfine and isotopic splitting. In order to find the differential abundances relative to the Sun, we made use of the integrated solar flux atlas of Kurucz et al. (1984) and derived the solar abundances for the same line list used for the targets. We assumed $T_{\text{eff}} = 5777$ K, $\log g = 4.44$ cgs, $\xi = 0.85$ km $^{-1}$ and calculated the solar model atmosphere by using Castelli & Kurucz (2003) grids. As described in §4.1, our line list has been slightly updated for the species that we determine abundances from *EW* measurements. Solar abundances for the updated lines are listed in Table 8 along with the ones derived by Asplund et al. (2009). For other lines that require synthetic spectrum matching technique, we adopted the abundances from Table 9 of Paper 1.

In this study, we used new transition probabilities for Co I (Lawler et al. 2015) and V I (Lawler et al. 2014), and so the solar Co and V abundances were re-calculated (Ta-

Table 8. Solar abundances. Species noted with (*) are updated abundances, the others are from Paper 1.

Species	$\log \epsilon_{\odot}$	$\log \epsilon_{\odot}$ (Asplund et al. 2009)
Li I	1.05±(0.05)	1.05±0.10
C	8.43±(0.05)	8.43±0.05
N*	7.99±(0.05)	7.83±0.05
O	8.69±(0.05)	8.69±0.05
Na I	6.34±(0.10)	6.24±0.04
Mg I	7.63±(0.16)	7.6±0.04
Al I	6.33±(0.18)	6.45±0.03
Si I*	7.55±0.06	7.51±0.03
Ca I*	6.32±0.06	6.34±0.04
Sc II		3.15±0.04
Ti I*	4.87±0.06	4.95±0.05
Ti II*	4.95±0.05	
V I*	3.87±0.03	3.93±0.08
Cr I*	5.60±0.05	5.64±0.04
Cr I*	5.70±0.07	
Mn I	5.41±(0.06)	5.43±0.04
Fe I*	7.42±0.06	7.50±0.04
Fe II*	7.41±0.05	
Co I*	4.92±0.07	4.99±0.07
Ni I*	6.26±0.07	6.22±0.04
Cu I	4.23±(0.10)	4.19±0.04
Zn I	4.51±(0.05)	4.56±0.05
Y II	2.23±(0.04)	2.21±0.05
La II	1.15±(0.06)	1.10±0.04
Nd II	1.39±(0.05)	1.42±0.04
Eu II	0.54±(0.08)	0.52±0.04

ble 8). We again relied on reverse solar analyses to derive the transition probabilities for Sc II lines that have no recent lab data. In Table 9 and Table 10 we list the derived abundances of all species $[X/\text{Fe}]$ for individual RGs and the mean cluster abundances ($\langle [X/\text{Fe}] \rangle$) of NGC 6940 and Hyades.

In total, we derived the abundances of 26 species of 23 elements. We will comment on a few of the computational issues and discuss the results by grouping the elements in the following nucleosynthetic groups; α (Mg, Si, Ca); light odd-Z (Na, Al); Fe-group (Sc, Ti, V, Cr, Mn, Fe, Co, Ni, Cu, Zn); *n*-capture (Y, La, Nd, Eu); and *p*-capture (Li, C, N, O). Figure 6 shows the abundances of all elements for the 12 RGs of NGC 6940 as listed in Table 9. The mean abundances of most species scattered around solar (0.01 to 0.1 dex).

6.1 α , Odd-Z, Fe-group and Neutron-capture elements

α and Odd-Z elements: We analyzed the α elements Mg, Si and Ca. Abundances of Si and Ca were derived from *EW* measurements of their neutral species. The cluster $\langle [\text{Si}/\text{Fe}] \rangle$ is slightly over solar while $\langle [\text{Ca}/\text{Fe}] \rangle$ is about solar (Table 9). Mg abundances were determined from synthetic spectrum fitting to the Mg lines at 5528.4 Å and 5711.1 Å; both lines are slightly contaminated by C₂ and CN molecular absorptions. $\langle [\text{Mg}/\text{Fe}] \rangle$ is solar (Table 9), as is the cluster mean of all three alphas:

$$\langle [\alpha/\text{Fe}] \rangle \equiv \frac{1}{3} ([\text{Mg}/\text{Fe}] + [\text{Ca}/\text{Fe}] + [\text{Si}/\text{Fe}]) = 0.06 \pm 0.07.$$

Abundance determination of two odd-Z light elements

Table 9. Elemental abundances of individual stars and average abundances ($\langle[X/Fe]\rangle$) for NGC 6940.

Species	MMU												$\langle[X/Fe]\rangle$	σ
[X/Fe]	28	30	60	69	87	101	105	108	132	138	139	152		
C	-0.29	-0.25	-0.38	-0.31	-0.29	-0.33	-0.34	-0.26	-0.39	-0.22	-0.29	-0.49	-0.32	0.07
N	0.19	0.19	0.23	0.26	0.19	0.25	0.19	0.37	0.21	0.24	0.16	0.34	0.23	0.06
O I	-0.15	-0.11	-0.25	-0.14	-0.12	-0.12	-0.20	-0.14	-0.27	-0.06	-0.12	-0.13	-0.15	0.06
Na I	0.06	0.06	0.01	0.07	-0.05	0.06	0.18	0.31	0.19	0.00	0.04	0.38	0.11	0.13
Mg I	-0.04	-0.08	-0.05	-0.04	-0.08	-0.02	0.01	0.09	0.01	-0.03	-0.05	0.05	-0.02	0.05
Al I	-0.02	-0.04	-0.07	0.03	-0.02	-0.03	0.04	0.16	0.05	0.00	0.00	0.12	0.02	0.07
Si I	0.10	0.13	0.00	0.11	0.07	0.12	0.17	0.13	0.20	0.05	0.13	0.21	0.12	0.06
Ca I	0.09	0.03	0.07	0.12	0.05	0.04	0.11	0.15	0.12	0.01	0.08	0.09	0.08	0.04
Sc II	-0.05	-0.03	-0.04	0.00	-0.07	0.04	-0.11	-0.08	-0.07	-0.03	-0.02	-0.04	-0.04	0.04
Ti I	-0.04	-0.06	-0.05	-0.06	-0.09	-0.06	-0.06	0.07	-0.01	0.01	-0.07	-0.01	-0.04	0.04
Ti II	-0.03	0.04	-0.03	-0.03	-0.04	0.01	-0.02	0.03	0.04	0.01	0.08	-0.03	0.00	0.04
V I	-0.04	-0.04	-0.09	-0.06	-0.12	-0.04	-0.06	0.04	-0.02	-0.01	-0.08	0.00	-0.04	0.04
Cr I	0.04	0.02	0.03	0.07	0.01	0.02	0.05	0.12	0.05	0.08	-0.01	0.06	0.04	0.03
Cr II	0.06	0.12	0.03	0.00	0.06	0.05	0.10	0.01	0.20	-0.01	0.09	0.04	0.06	0.06
Mn I	-0.11	-0.12	-0.13	-0.13	-0.16	-0.13	-0.20	-0.09	-0.06	-0.11	-0.15	-0.06	-0.12	0.04
[Fe I/H]	0.05	0.09	0.12	0.05	0.14	0.09	-0.02	-0.07	0.07	0.08	0.09	0.02	0.06	0.06
[Fe II/H]	0.02	0.05	0.10	0.03	0.12	0.07	-0.06	-0.13	0.01	0.04	0.07	-0.04	0.02	0.07
Co I	-0.12	-0.08	-0.15	-0.13	-0.17	-0.09	-0.12	-0.09	-0.09	-0.10	-0.11	-0.05	-0.11	0.03
Ni I	-0.02	-0.02	-0.04	-0.02	-0.03	-0.01	0.01	-0.03	-0.01	-0.02	0.03	0.01	-0.01	0.02
Cu I	-0.10	-0.03	-0.14	-0.13	-0.16	-0.10	-0.16	-0.11	-0.05	-0.08	-0.07	0.02	-0.09	0.05
Zn I	0.06	0.07	0.09	0.08	0.00	0.08	0.17	0.04	0.09	0.04	0.18	0.03	0.08	0.05
Y II	0.00	0.02	-0.05	-0.01	-0.06	0.02	-0.05	0.07	-0.07	-0.04	0.03	0.00	-0.01	0.04
La II	0.04	0.10	-0.03	0.08	0.03	0.14	0.00	0.06	0.04	0.09	0.06	0.05	0.05	0.05
Nd II	0.19	0.24	0.15	0.15	0.22	0.26	0.15	0.12	0.16	0.15	0.17	0.23	0.18	0.04
Eu II	-0.06	0.03	-0.01	0.01	-0.04	0.03	0.01	0.01	-0.02	0.07	0.02	0.01	0.00	0.03
[N/C]	0.48	0.44	0.61	0.57	0.48	0.58	0.53	0.63	0.61	0.46	0.45	0.83		
log ϵ (Li)	1.05	< 0	1.23	1.29	0.56	0.64	< 0.1	< 0	0.33	1.05	0.86	< 0		

Na and Al were made via synthetic spectra. Na I lines at 5682.6, 5688.2, 6154.2 and 6160.8 Å were analyzed; the Na D lines were far too strong to be useful. According to Takeda et al. (2003) the Na lines we analyzed are mildly affected by non-LTE in disk stars. Their calculations indicate that non-LTE corrections are quite small and about -0.1 and -0.05 dex for 5682/5688 and 6154/6160 absorption lines, respectively. These non-LTE correction factors are small enough that we chose not to apply them to our results.

The mean Na abundance for the cluster is $\langle[Na/Fe]\rangle = 0.11 \pm 0.13$. Na abundances in MMU 108 and MMU 152, depart from the solar abundance by about 0.3 dex and 0.4 dex, respectively. Possible reasons for the differences in Na abundances will be discussed in §7. Al abundances of the stars were determined from four Al I lines; 6696.1, 6696.7, 7835.3 and 7836.1 Å; all are blended by atomic lines and thus needed synthetic spectrum treatment. The mean cluster abundance of this element is solar: $\langle[Al/Fe]\rangle = 0.02 \pm 0.07$. The Al abundances of MMU 108 and MMU 152 also depart from the solar abundance by about ~ 0.14 dex. Deviation of the Na and Al abundances of these RGs from the mean can be seen in Figure 6.

Fe-group elements: Abundances of Ti, Cr, and Ni were treated to single-line *EW* analyses, all of which yielded $\langle[X/Fe]\rangle \simeq 0$ (Table 9, Figure 6). Ti abundances from Ti I and Ti II lines have already been considered as part of model atmosphere determinations (§5.2). We used 7–10 Ti I and 2–4 Ti II lines for each star. For Cr, 6–13 Cr I lines and 2–3 Cr II lines were employed. We used up to 21 neutral Ni I

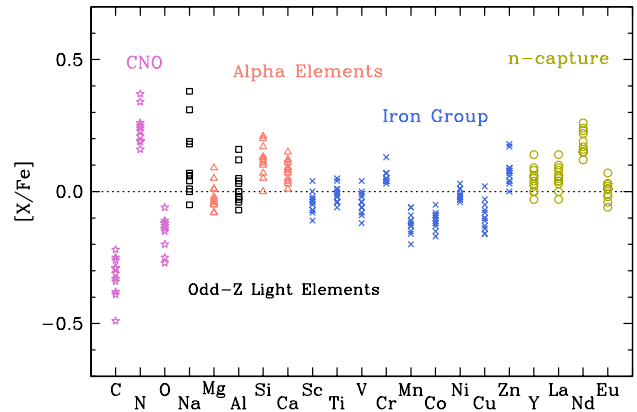


Figure 6. $[X/Fe]$ values of the species studied for the entire RG sample. Dotted line represents the solar values. Abundances of CNO, odd-Z, alpha, iron-group and n-capture elements are shown by stars, squares, triangles, crosses and empty circles, respectively.

lines for the abundance determinations. The abundances of Ti, Cr, and Ni appear to be very well determined.

We used the MOOG *blends* option to derive abundances from uncontaminated but hyperfine-split transitions of Sc II, V I, and Co II. The mean cluster abundances of Sc and V are almost exactly solar, while Co appears to have a small underabundance (Table 9).

Abundances of the remaining Fe-group elements were determined by synthetic spectrum matching. As discussed in §4.1 we analyzed three Mn I lines located around 6016 Å.

Table 10. Elemental abundances of individual stars and average abundances ($\langle[X/Fe]\rangle$) for Hyades.

Species [X/Fe]	δ Tau	ε Tau	γ Tau	θ Tau	$\langle[X/Fe]\rangle$	σ
C	-0.49	-0.45	-0.42	-0.44	-0.45	0.03
N	0.33	0.37	0.44	0.36	0.38	0.04
O I	-0.28	-0.19	-0.20	-0.15	-0.20	0.06
Na I	0.21	0.18	0.23	0.14	0.19	0.04
Mg I	-0.01	0.00	-0.04	-0.10	-0.04	0.04
Al I	0.04	0.09	0.07	0.01	0.05	0.03
Si I	0.27	0.26	0.22	0.21	0.24	0.03
Ca I	0.08	0.03	0.06	0.02	0.05	0.03
Sc II	-0.02	0.04	-0.01	0.09	0.02	0.05
Ti I	-0.09	-0.08	-0.03	-0.01	-0.05	0.04
Ti II	-0.05	-0.01	0.05	0.05	0.01	0.05
V I	-0.09	-0.02	0.01	-0.01	-0.03	0.04
Cr I	0.06	0.05	0.04	0.03	0.04	0.01
Cr II	0.12	0.22	0.14	0.12	0.15	0.05
Mn I	-0.14	-0.14	-0.13	-0.18	-0.15	0.02
[Fe I/H]	0.08	0.14	0.12	0.15	0.12	0.03
[Fe II/H]	0.07	0.11	0.12	0.16	0.12	0.04
Co I	-0.09	-0.06	-0.04	-0.04	-0.06	0.02
Ni I	0.01	0.06	0.03	0.07	0.04	0.03
Cu I	-0.07	-0.05	-0.04	-0.07	-0.06	0.01
Zn I	0.08	-0.04	0.00	0.00	0.01	0.05
Y II	-0.14	-0.09	-0.17	-0.17	-0.14	0.04
La II	-0.12	-0.07	-0.09	-0.02	-0.07	0.04
Nd II	0.07	0.16	0.15	0.11	0.12	0.04
Eu II	-0.14	-0.08	-0.11	-0.03	-0.09	0.05
[N/C]	0.82	0.83	0.86	0.80		
$\log \epsilon(\text{Li})$	0.87	0.54	0.97	1.11		

The mean cluster abundance is somewhat subsolar: All RGs slightly deficient in Mn; the abundance mean is $\langle[\text{Mn}/\text{Fe}]\rangle = -0.12$ ($\sigma = 0.04$). The Cu abundance of the cluster, based only on the 5782 Å transition (§4.1), is only marginally subsolar (Table 9). We also derived the Zn abundance using the neutral Zn line located at 6362.3 Å. This absorption line is contaminated by CN, Sc and V, which makes an accurate abundance determination difficult for Zn. Star-to-star Zn abundance scatter can be seen in Table 9, but the abundance mean is only slightly in excess of solar.

Neutron-capture elements: Abundances of all n-capture elements were determined by spectrum synthesis. We derived abundances of s-process (slow neutron-capture) elements Y, La and Nd, and also one r-process (rapid neutron-capture) element Eu. For Y and La we derived solar abundances (Table 9) from our spectrum analyses of the lines listed in Table 4. Nd abundances were derived from three Nd lines (5249.6, 5293.2 and 5319.8 Å) in most cases, leading to the largest departure from solar abundances of elements that do not participate in H-burning: $\langle[\text{Nd}/\text{Fe}]\rangle = +0.18$ ($\sigma = 0.04$). The lines of the r-process element Eu used for the abundance analysis are Eu II 6645.1 and 7217.5 Å. For some RGs we could not use 7217.5 Å line since its strength is small and disappears in the continuum. An example for synthetic-observed spectra comparison is given in Figure 7 for the Eu II 6645.1 and La II 6262.3 Å regions of MMU 152. The figure contains three synthesis with 0.3 dex steps and abundances are in $\log \epsilon$ unit. Red solid line in the middle represents the best fit and the abundance accepted

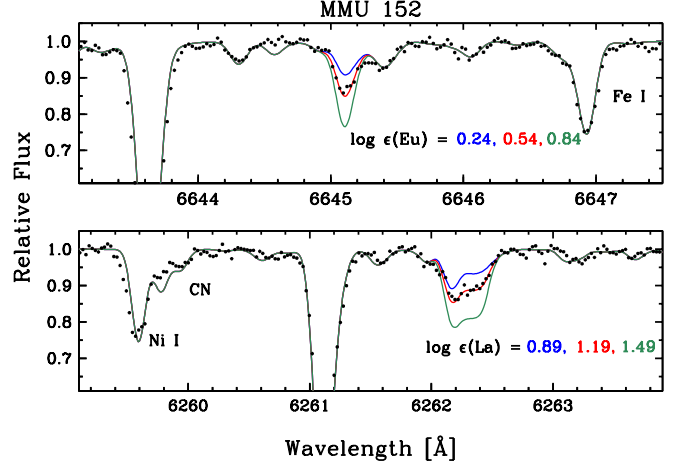


Figure 7. Observed spectra (filled circles) and synthetic spectra (lines) of the Eu II 6645 Å line (top panel) and the La II 6262 Å lines in MMU152. Assumed abundances for the synthetic spectra are written in the figure panel legends. The synthesis that best matches the observed spectrum is the red line; syntheses for abundances smaller and larger than this value by 0.3 dex are displayed with blue and green lines, respectively.

for this star. The individual Eu abundances among all listed RGs are in agreement and the mean Eu abundances for the cluster is solar (Table 9).

Recent study of Blanco-Cuaresma et al. (2015) investigates the chemical abundances of 14 elements (Na, Mg, Si, Ca, Sc, Ti, V, Cr, Mn, Fe, Co, Ni, Y, Ba) for one RG member of NGC 6940. We have 13 elements that are common with the sample of Blanco-Cuaresma et al.. All are in good agreement with their findings except for the abundances of [Na/Fe], [Mn/Fe] and [Co/Fe], which are away from our findings by 0.14 dex, 0.14 dex and -0.13 dex, respectively.

6.2 Light elements

LiCNO abundances were derived by spectrum synthesis. C, N, and O are bound together through the molecules such as CN, CH and CO. Therefore, we performed iterative syntheses to derive their abundances. As discussed in Paper I, we used recent molecular laboratory data in analyses of the C₂ and CN bands. First we derived O abundances using the non-LTE free [O I] 6300.3 Å forbidden line. Then C abundances were determined from C₂ Swan bandheads at 5160 Å and 5631 Å, adopting the new O abundances. These steps were repeated until the changes in O and C abundances were negligible between iterations. Finally, with these abundances we analyzed the 7995-8040 Å region using ¹²CN and ¹³CN red system lines to derive N abundances and carbon isotopic ratios.

A concern for the O analysis is the relatively small radial velocity shift of NGC 6940 (Table 3), which potentially can lead to contamination of the stellar [O I] 6300 Å line by its night-sky emission counterpart. We also tried to derive O abundances from the [O I] 6363 Å without much success: this line is very weak, contaminated by stellar CN features, and very much distorted by its night sky emission. Figure 8 shows the best (upper panel) and worst (lower panel) case scenario for the 6300 Å situation. We decided not to at-

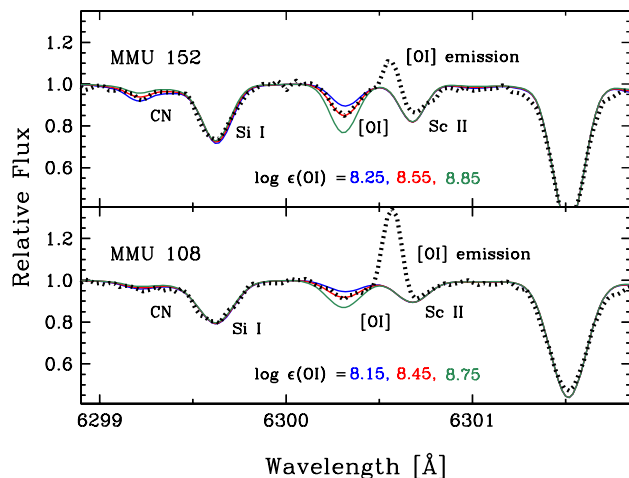


Figure 8. Observed and synthetic spectra of the [O I] line in MMU 152 (top panel) and MMU 108 (bottom panel). The symbols and lines have the same meanings as in Figure 7.

tempt removal of the night sky components in order not to risk damaging the [O I] absorption lines. In Figure 8 we compare the observed spectra of MMU 152 and MMU 108 with synthetic spectra. The synthetic spectrum represented with red solid line is the best fit. Blue and green solid lines represent the analysis ± 0.3 dex away from the best fit. All of our programme RGs are slightly or moderately affected by the night sky emission line. Since the night sky emission line is more blended with 6300.68 Å [Sc II] line, we mainly focused on the blue side of the [O I] to obtain more reliable O abundances. We also took into account the CN 6300.27 Å and Ni I 6300.34 Å (Johansson et al. 2003) contributions to the [O I] 6300.31 Å line.

The derived O abundances of NGC 6940 RGs indicate some star-to-star scatter, from [O/Fe] = -0.27 (MMU 132) to -0.06 (MMU 138). Clearly the reader should keep in mind that the night sky emission contamination may increase the uncertainty in our O abundances. The mean for the cluster is [O I/Fe] = -0.15 ($\sigma = 0.06$). Note that similar O underabundances were also observed among NGC 752 members (Paper 1), and that cluster’s radial velocity safely distances the stellar and night-sky 6300 Å lines.

Carbon abundances were derived from C₂ Swan system features in two regions: the (0-0) bandhead at 5165 Å and (0-1) bandhead at 5635 Å. Our spectral coverage does not include CH G-band 4300 Å region, so we were not able to use CH to check our C₂ results. The complex structure of the C₂ bands, which are severely blended atomic absorption features in the 5165 Å region and are very weak in the 5635 Å region, bring difficulties in determination of C abundances. In Figure 9, we show an example spectral synthesis of both Swan regions for MMU 101. The red solid line represents the best fit to the observed spectrum, and blue and green solid lines represent the -5 and $+0.3$ dex departure from the best fit respectively. C abundances obtained from 5165 Å bandhead are lower compared to those obtained from 5635 Å, the mean difference being ~ 0.17 dex. The averages of these two regions were adopted as the final carbon abundances, which are given in Table 9. All C abundances are subsolar, ranging from [C/Fe] = -0.49 (MMU 152) to -0.22 (MMU 138),

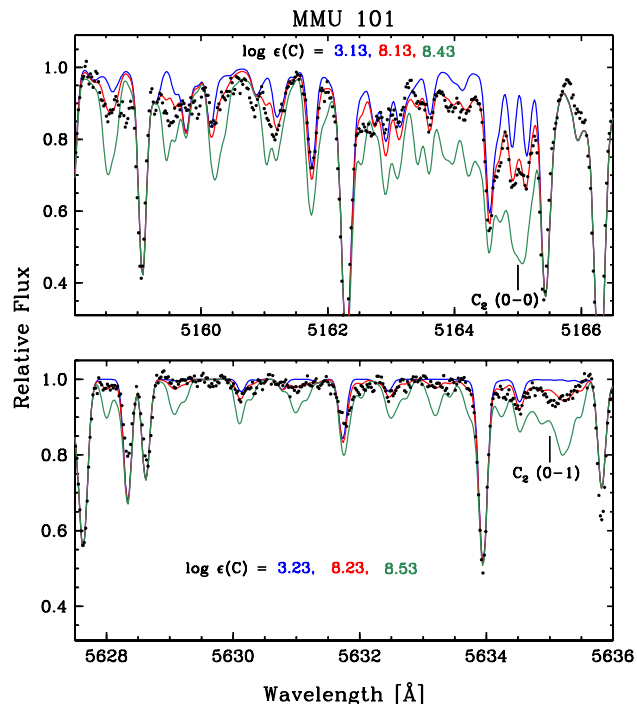


Figure 9. Observed and synthetic spectra of the C₂ Swan system (0-0) bandhead (top panel) and (0-1) bandhead (bottom panel) in MMU 101. The symbols and lines have the same meanings as in Figure 7.

leading to the mean $\langle [C/Fe] \rangle = -0.32$, with only modest star-to-star scatter ($\sigma = 0.07$).

Nitrogen abundances were derived using ¹²CN features in the 7995–8040 Å region. All of the RG members in our list are overabundant in nitrogen. Figure 10 shows the spectrum synthesis for the most N-enhanced NGC 6940 member MMU 108, which has [N/Fe] = $+0.37$. The best fit to the observed spectrum (black dots) is represented by a red solid line in both panels. The average N abundance for this star is $\log \epsilon(N) = 8.26$. The mean N abundance for the cluster is $\langle [N/Fe] \rangle = +0.23$ ($\sigma = 0.06$).

One of our main goals is to derive ¹²C/¹³C ratios, which are sensitive indicators of stellar interior light element synthesis and envelope mixing in RG stars. There are several ¹²CN and ¹³CN features that can be used to derive ¹²C/¹³C in the ~ 8000 –8048 Å region. However, due to atomic and molecular line blending, we concentrated on analyses of the prominent ¹²CN lines at 8003 Å and ¹³CN lines at 8004 Å and used the strengths of weaker ¹³CN lines as corroborating evidence. In Figure 11, we display the spectral region surrounding these CN lines in three different RGs. These stars are representative of the ¹²C/¹³C range of our NGC 6940 RGs; see Table 11. As seen in Table 11, seven cluster members have ¹²C/¹³C values in the 20–25 range, as predicted from standard first dredge-up (FDU) theory for RGB stars. However, four NGC 6940 program stars have values lower than expected, 10–15. The most interesting RG is MMU 152 (see the bottom panel of Figure 11), which has ¹²C/¹³C = 6.

Li abundances were derived from the neutral Li resonance doublet at 6707.8 Å. Our syntheses took into account its hyperfine structure, and also the blending with 6707.4 Å Fe I line. In Figure 12 we have plotted the Li region for three

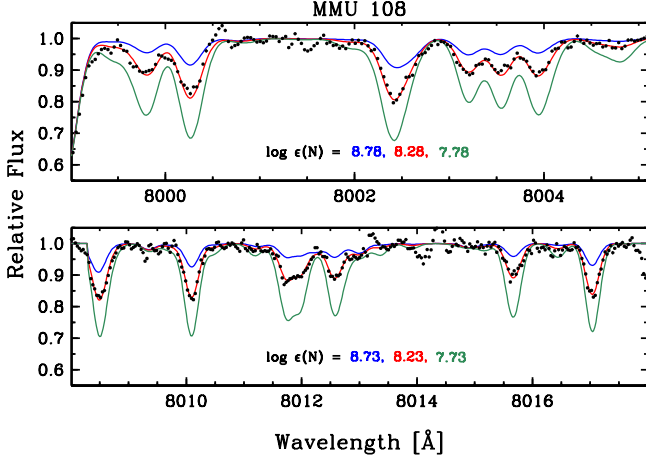


Figure 10. Observed and synthetic spectra of CN transitions in 7999–8005 Å (top panel) and the 8008–8017 Å (bottom panel) wavelength regions in MMU 108. The symbols and lines have the same meanings as in Figure 7.

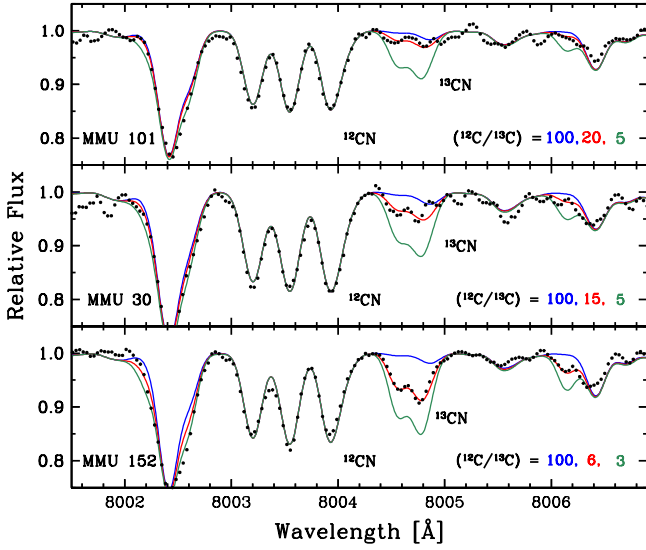


Figure 11. Observed and synthetic spectra of CN transitions in 8001–8007 Å wavelength region in three stars with different carbon isotopic ratios. This spectral interval is shown to highlight the prominent ^{13}CN 8004 Å triplet, which is often the key $^{12}\text{C}/^{13}\text{C}$ ratio indicator in RGs. The symbols and lines have the same meanings as in Figure 7.

RG members. These stars represent the member-to-member Li abundance variation in our NGC 6940 sample. Li abundances of all the RGs are listed in Table 9. MMU 69 has the most enhanced Li abundance among all of our targets: $\log \epsilon(\text{Li}) = 1.29$. There are no Li detections for four of the RG members.

6.3 Abundances in the Hyades

Derivation of atmospheric parameters and abundances of the four Hyades RGs have been described in §5 and §6. These were accomplished with the same methods that were applied to the NGC 6940 RGs, and the results are entered in Tables 6, 10 and 11.

Table 11. Carbon isotopic ratios.

Star	$^{12}\text{C}/^{13}\text{C}$	σ
MMU 28	20	−5 / +5
MMU 30	15	−3 / +3
MMU 60	20	−3 / +5
MMU 69	10	−5 / +5
MMU 87	25	−5 / +5
MMU 101	20	−5 / +5
MMU 105	15	−2 / +3
MMU 108	20	−3 / +5
MMU 132	20	−5 / +5
MMU 138	12	−2 / +3
MMU 139	13	−3 / +2
MMU 152	6	−1 / +2
δ Tau	25	−2 / +2
ϵ Tau	26	−1 / +4
γ Tau	25	−2 / +2
θ Tau	27	−2 / +3

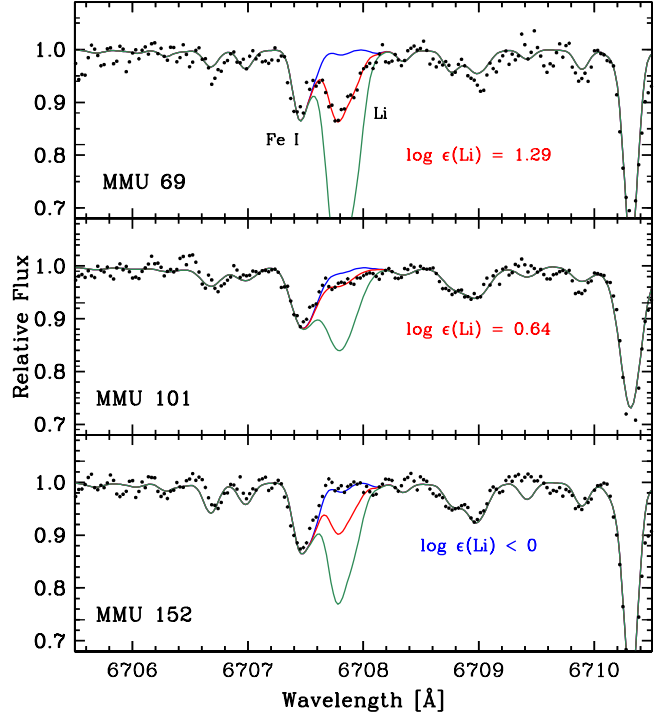


Figure 12. Observed and synthetic spectra of the Fe I 6707 Å resonance doublet in three stars with contrasting Li abundances. The symbols and lines have the same meanings as in Figure 7.

The Hyades metallicity determined by our methods is $\langle [\text{Fe I}/\text{H}], [\text{Fe II}/\text{H}] \rangle = +0.12$, slightly larger than our value for NGC 6940, $\langle [\text{Fe I}/\text{H}], [\text{Fe II}/\text{H}] \rangle = +0.04$. This is in good accord with many previous studies that have found the Hyades to be more metal-rich than the Sun. For example, $\langle [\text{Fe}/\text{H}] \rangle = +0.16$, $\sigma = 0.02$ (Liu et al. 2016), $+0.15$, $\sigma = 0.06$ (Maderak et al. 2013, unweighted mean), $+0.21$, $\sigma = 0.07$ (Smiljanic 2012), $+0.22$, $\sigma = 0.05$ (Schuler et al. 2006), $+0.12$, $\sigma = 0.02$ (Carrera & Pancino 2011), $+0.13$, $\sigma = 0.05$ (Paulson et al. 2003), and earlier studies that are cited in these papers.

The relative $[\text{X}/\text{Fe}]$ values of Hyades giants determined

Table 12. Updated NGC 752 abundances.

Species	1	3	11	24	27	MMU 77	137	295	311	1367	$\langle[X/Fe]\rangle$
[N/Fe] ^a	0.29	0.22	0.24	0.28	0.32	0.27	0.28	0.28	0.27	0.25	0.27 ± 0.03
[Mn I/Fe]	-0.18	-0.19	-0.21	-0.18	-0.15	-0.15	-0.18	-0.21	-0.21	-0.16	-0.18 ± 0.03
[Cu I/Fe]	-0.14	-0.19	-0.17	-0.14	-0.05	-0.10	-0.07	-0.08	-0.16	-0.15	-0.12 ± 0.05
[Y II/Fe]	-0.04	-0.11	-0.10	-0.08	-0.04	-0.02	-0.03	-0.06	-0.13	-0.16	-0.08 ± 0.05
[Nd II/Fe]	0.20	0.15	0.15	0.08	0.22	0.28	0.23	0.22	0.17	0.12	0.18 ± 0.06

^a Only solar abundance updated.

in this study are nearly identical to those of NGC 6940 and NGC 752. Computing the mean difference of the entries in Tables 9, 10, 12 and Table 10 in Paper 1, we find $\langle[X/Fe]_{NGC6940} - [X/Fe]_{Hyades}\rangle = 0.00 \pm 0.02$ ($\sigma = 0.08$). Doing a similar comparison of the Hyades to NGC 752 (Paper I, Table 10) yields a similar agreement: $\langle[X/Fe]_{NGC752} - [X/Fe]_{Hyades}\rangle = -0.02 \pm 0.02$ ($\sigma = 0.08$). This general abundance ratio accord among the three clusters is apparent in the $[X/Fe]$ values displayed in Figure 13.

There are few comprehensive chemical composition studies of Hyades giants in the literature. Of recent studies, Carrera & Pancino (2011) includes the most elements in common with our work. In general our Hyades abundances are in good accord with theirs: $\langle[X/Fe]_{Carrera} - [X/Fe]_{us}\rangle = -0.01 \pm 0.02$ ($\sigma = 0.08$, for 16 species in common). Lambert & Ries (1981), one of the first large-sample surveys of light elements in RGs, included the four Hyades stars. Forming abundance differences for individual stars in the sense Lambert & Ries *minus* this study, and computing 4-star means, we find $\Delta[Fe/H] = -0.02$ ($\sigma = 0.04$), $\Delta[C/Fe] = +0.16$ ($\sigma = 0.04$), $\Delta[N/Fe] = +0.01$ ($\sigma = 0.03$), and $\Delta[O/Fe] = +0.15$ ($\sigma = 0.04$). Caution is warranted in this comparison, given the improvements in stellar atmosphere modeling and atomic/molecular linelists over the last few decades, and with our more extensive spectral coverage of the C₂ Swan bands compared to the earlier study. We suspect that the larger O abundances of Lambert & Ries may be due to the influence of the Ni I contamination of the 6300 Å [O I], which was not understood at the time of the Lambert & Ries study. Their C abundances are somewhat larger than ours, but their N abundances are in good accord. Lambert & Ries quote carbon isotopic ratios from earlier papers in their series (e.g. Tomkin et al. 1976), which are on average somewhat lower than ours: $\Delta^{12}C/^{13}C = -5$ ($\sigma = 2$). Their values should generally be more accurate than ours since they used more CN features in their work than done here. More detailed comparisons are beyond the scope of our work here.

7 SUMMARY AND DISCUSSION

This study is the second in this series of papers on the chemical compositions RGs of OCs. Here we report the first detailed chemical abundance analysis of NGC 6940, giving results for 12 RG members. In Paper 1 we studied 10 RG members of the open cluster NGC 752 in the same man-

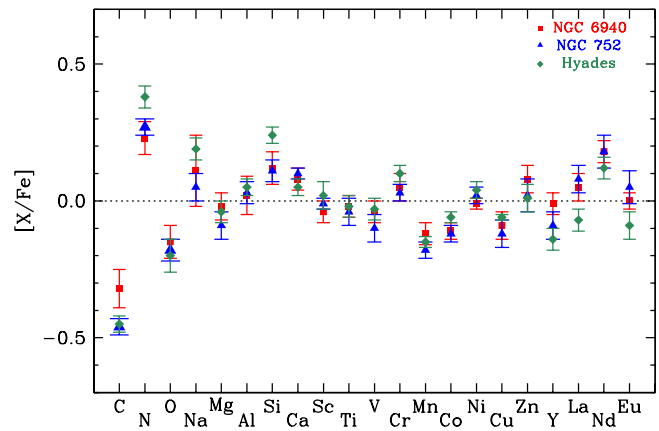


Figure 13. Abundance ratios in the three OCs studied in this work and in Paper I. The point types and colors are identified in the figure legend.

ner. Our main focus for these two studies is to derive the abundances of light (LiCNO) elements and $^{12}C/^{13}C$ ratios.

We first confirmed NGC 6940 membership of our 12 program stars via RV calculations from our spectra. By applying the Y² isochrones to Larsson-Leander (1960) photographic observations we then estimated the turn-off mass ($\approx 2 M_{\odot}$) and age (~ 1.1 Gyr) of the cluster. The turn-off mass was assumed to apply to the RG masses. Then with the known cluster reddening, distance modulus, colors and spectroscopic line depth ratios, we calculated initial model atmosphere parameters. We iteratively applied standard spectroscopic line analysis techniques to iterate to achieve final model atmosphere parameters T_{eff} , $\log g$, ξ_t and $[M/H]$. The mean metallicity for the NGC 6940 was found to be about solar, $\langle[M/H]\rangle = -0.06 \pm 0.07$.

We then derived the abundances of a number of light (Li, C, N, O), odd-Z (Na, Al), α (Mg, Si, Ca), Fe-group (Ti, Cr, Ni, Mn, Cu, Zn), n-capture elements (Y, La, Nd, Eu) and also determined the $^{12}C/^{13}C$ isotopic ratios of the RGs. The overall abundance pattern of the NGC 6940 members are mostly around solar (Figure 6). For some of the species, such as Na, line-to-line scatter among individual RGs is a bit higher compared to others. This is either due to lack of recent lab data or complex hyperfine structures of these species. Along with the RG members of NGC 6940 (1.1 Gyr), we also analyzed the four well-known RG members of the Hyades (0.63 Gyr) open cluster with the aim of standardizing and showing the reliability of the method we

use for the analysis of the open cluster NGC 6940. Hyades RGs have been a subject of many studies. Our derived atmospheric parameters and elemental abundances of Hyades RGs as listed in Table 6 and Table 10, respectively. Our results are generally in good agreement with the literature. We also give the overall comparison of the abundances in NGC 6940, NGC 752 and Hyades open clusters in Figure 13. Some deficiency in neutron-capture elements Y, La and Eu and a slight enhancement in Si abundance are noticeable in Hyades open cluster when compare to NGC 6940 and NGC 752. Other elements mostly behave similarly.

7.1 Evolutionary Status of the RGs

NGC 6940 is an intermediate age open cluster with an age of 1.1 Gyr suggested by Y^2 isochrone fits to its CMD (Figure 1). The LiCNO abundances and $^{12}\text{C}/^{13}\text{C}$ ratios of the RGs we investigate in this study indicate that although these stars are the members of the same OC, they must have experienced different types/amounts of mixing during their giant branch evolution. In our sample, we have six RGs that have $^{12}\text{C}/^{13}\text{C} < 20$, lower than predicted by canonical models: MMU 30, 69, 105, 138, 139 and 152 (Table 11). Four of the RGs have no sign of Li in their spectra: MMU 30, 105, 108 and 152 with $^{12}\text{C}/^{13}\text{C} = 15, 15, 20$ and 6, respectively. In the next two subsections we will discuss the general features of Li, $^{12}\text{C}/^{13}\text{C}$, [N/C] and Na abundances in NGC 6940, but we call attention here the results for two of our stars. MMU 152 stands out in a need for an extra-mixing process. MMU 108 has the highest T_{eff} among other RGs with no sign of Li and $^{12}\text{C}/^{13}\text{C} = 20$. Similarly, other members with low $^{12}\text{C}/^{13}\text{C}$ ratios might have experienced extra-mixing processes at different levels and started He-burning in their cores. As first suggested by Cannon (1970), a clump of red giants centred near $M_{V_0} = +1$ and $(B - V)_0 = 1$ in the general field are probably core helium burning horizontal branch stars. The mean absolute magnitude and intrinsic colour for the RG members of NGC 6940 in our sample are $\langle M_{V_0} \rangle = 1.12$ ($\sigma = 0.32$) and $\langle (B - V)_0 \rangle = 0.90$ ($\sigma = 0.06$), suggesting all the RGs investigated here reside at the clump region. Most of the sample seem to locate closer to the bluer part of the RC, which is generally called the red horizontal branch (RHB) (e.g. Kaempf et al. 2005), indicating the slight initial mass differences between the members.

7.2 LiCNO

The so-called FDU mechanism alters surface abundances as stars evolve up the RGB. During this episode, the convective envelope of a star deepens towards inner regions and brings the chemically processed material to the surface. This mixing causes surface abundance changes in RGs: typically [N/Fe] increases by about 0.4 dex, [C/Fe] decreases by about 0.20 dex, and O abundance remains around solar (e.g. §2.2 in Karakas & Lattanzio 2014). The $^{12}\text{C}/^{13}\text{C}$ isotopic ratio also changes during the FDU, dropping from its main sequence value (~ 90) to 20–30. The He abundance increases by $\Delta Y \approx 0.012$ (unobservable). The main isotope of Li, ^7Li , is destroyed by H burning at relatively low temperatures ($T \geq 2.5 \times 10^6$ K). Therefore, its surface abundance also alters during the FDU and drops to

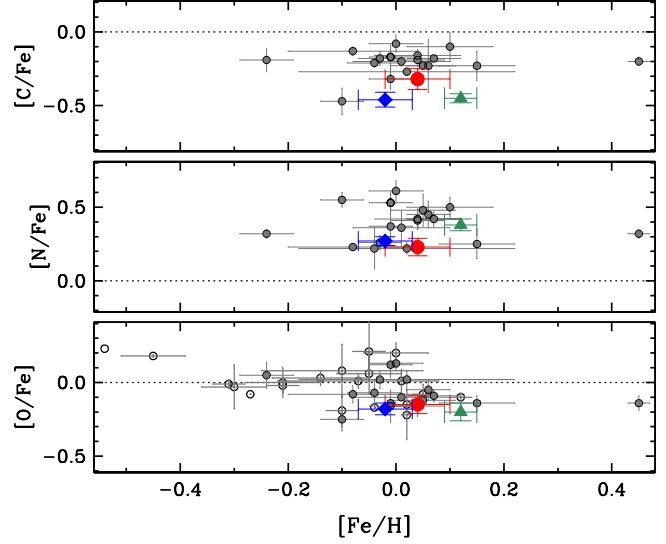


Figure 14. Comparison of CNO abundances with the literature. Red dots are NGC 6940, blue diamonds are NGC 752 while green triangles are Hyades. Grey dots (Smiljanic et al. 2009; Tautvaišienė et al. 2000; Tautvaišienė et al. 2005, 2015; Mikolaitis et al. 2010, 2011a,b, 2012; Santrich et al. 2013; Zacs et al. 2011) represents OCs from the literature and open circles (Friel et al. 2005, 2010; Jacobson et al. 2008, 2009a, 2011a; Pancino et al. 2010; Yong et al. 2005) are O abundances derived without C and N abundances.

$\log(\epsilon)(\text{Li}) \simeq 1$ (Karakas & Lattanzio 2014). Besides the elements mentioned above, FDU has minor effects on the other elements (see Karakas & Lattanzio 2014, and references therein).

Li is a fragile element with short lifetime in H-burning zones. Its surface abundance is known to be very sensitive to mixing processes, thus can vary greatly among RG stars. The complex behaviour of Li has been studied by many authors for decades. For example, Palmerini et al. (2011) investigated the Li abundance problem in low-mass ($\leq 3 M_{\odot}$) solar metallicity red giants. They applied several theoretical models that involve deep-mixing mechanisms to the observational data. They concluded that different set of deep-mixing mechanisms can cause different amount of Li abundances lower than $A(\text{Li}) = 1.5$ after the FDU. Their models do not predict any further mixing after the luminosity function bump, during which H-burning shell erases the chemical discontinuity left by the FDU. Results of the mixing at different depths are shown in Figures 1 and 4 of Palmerini et al. (2011). Our sample has a Li abundance range from $0 < A(\text{Li}) < 1.3$. Assuming that the theoretical timescales for first-ascent giants are in good agreement with the observations, the average temperature of the RGs in our sample along with the turn-off mass of the NGC 6940 strongly suggest that our RGs reside at the clump region predicted in Palmerini et al. (2011). In another recent study, Charbonnel & Lagarde (2010) discuss how the thermohaline and rotation-induced mixing modify the surface abundances in giant stars. Their model predictions indicate that, for a star with initial mass of $2 M_{\odot}$, depending on the mixing mechanisms (thermohaline instability and/or rotation-induced mixing) involved at the end of the FDU, Li abundances can change from about the canonical value of

1.4 to <0 (Figure 14 in Charbonnel & Lagarde 2010). The Li abundance diversity in our sample appears to be a very good implication of the different mixing mechanisms taking place in stellar interiors.

The mean CNO abundances we obtained for the NGC 6940 are $[C/Fe] = -0.32 \pm 0.07$, $[N/Fe] = +0.23 \pm 0.06$, $[O/Fe] = -0.15 \pm 0.06$, which are in general agreement with the standard mixing theories summarized above. In Figure 14, we compare our CNO abundances with other RGs in different OCs studied in the literature. In this figure grey dots represent the average abundance ratios of those RGs. In the bottom panel of the Figure 14 open circles represent the O abundances derived without C and N abundances. The average CNO abundance ratios of the NGC 6940, NGC 752 and Hyades are illustrated by red dot, blue diamond and green triangle, respectively. The error bars indicate the standard deviation of the mean abundances. As is seen in this figure, our CNO abundances agree fairly well with the data from other open clusters. Emphasis on the usage of different solar abundances in these studies should be made. For example, solar CNO abundances we used in our study (Table 8) are 8.43, 7.99 and 8.69, respectively. Other authors, however, usually prefer to adopt the solar abundances from Grevesse & Sauval (1998), in which the solar CNO abundances are given as 8.52, 7.92, 8.83, or from Grevesse et al. (2007) that reports abundances as 8.39, 7.78 and 8.66, respectively. These differences, in general, create small offsets that affect the comparisons of abundance ratios.

Theoretical models predict that post dredge-up $[N/C]$ values increase with initial stellar masses (Charbonnel & Lagarde 2010). Derived $[N/C]$ values in our clusters are moderately in accord with the predictions of Charbonnel & Lagarde (2010). Average $[N/C]$ values of the clusters are $[N/C]_{\text{NGC 6940}} = 0.56 \pm 0.11$, $[N/C]_{\text{NGC 752}} = 0.73 \pm 0.04$ and $[N/C]_{\text{Hyades}} = 0.83 \pm 0.02$. Since our C and N abundances were determined in the same way for these three clusters, their relative N/C ratios may be more robust than derived values for individual stars in individual clusters. We may attempt to interpret these relative abundances in terms of theoretical predictions discussed in Charbonnel & Lagarde (2010) and Karakas & Lattanzio (2014).

$[N/C]$ ratios among the giant members of NGC 6940 have a significant range from 0.44 to 0.83. MMU 30 has the lowest $[N/C]$ value with 0.44 and has $^{12}\text{C}/^{13}\text{C} \simeq 15$. Evaluating these parameters together with the turn-off mass of the cluster in Figure 17, 19 and 20 of Charbonnel & Lagarde (2010) suggests that thermohaline mixing is the major mechanism that leads to these values, perhaps along with a slightly high initial rotational velocity. On the other hand, MMU 152 with $[N/C] = 0.83$ and $^{12}\text{C}/^{13}\text{C} \simeq 6$ exhibits a unique behaviour. Comparing its values with the model predictions indicates a mixing mechanism mainly governed by a very high initial rotational velocity ($V_{\text{ZAMS}} > 300 \text{ km s}^{-1}$) that might also imply a higher initial mass. Diversity in $[N/C]$, $^{12}\text{C}/^{13}\text{C}$ ratios and Na abundances (discussed below) suggests that, although the cluster members have started of similar initial chemical compositions, perhaps different initial masses distribution of the members prompted different mixing mechanisms.

The mean $[N/C] = 0.73$ of NGC 752 suggests a contribution by rotation-induced mixing. Different $^{12}\text{C}/^{13}\text{C}$ ratios

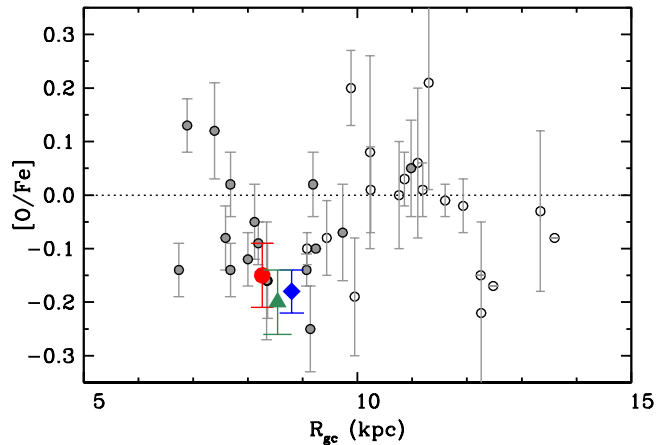


Figure 15. Galactocentric radial distribution of $[O/Fe]$ abundances. Symbols are the same as in Figure 13.

among the cluster members (Paper 1) imply the existence of a dominant thermohaline mixing mechanism in some cases. Evolved members of Hyades have more depletion in carbon (previously noticed by Schuler et al. 2009) compared to NGC 752 and NGC 6940. The average $[N/C] = 0.83$ value of Hyades suggests higher initial masses and rotation-induced mixing with relatively high initial velocities. $^{12}\text{C}/^{13}\text{C}$ values, on the other hand, are in accord with the standard models. Our interpretation on the mechanisms that lead to extra-mixing in RGs are based on various parameters and need to be taken with caution.

The elemental abundances we derived for the RGs of Hyades agree well with the literature (e.g. Carrera & Pancino 2011) but some discrepancies arise for a few elements. For example, oxygen is generally found around solar in most cases but our sub-solar oxygen abundances are only in accord with Carrera & Pancino (2011). Sub-solar oxygen abundances seem to be a common issue among the giant members of NGC 6940, NGC 752 and Hyades (Figure 13 and Figure 15). On average, the oxygen abundance in these clusters is subsolar about 0.2 dex. A simple explanation to this deficiency is that these clusters, which have galactocentric distances between $8.2 < R_{\text{GC}} < 8.8 \text{ kpc}$, might have formed from molecular clouds with initially low oxygen abundances. In Figure 15 we plot O abundance as a function of Galactocentric distance for the same clusters that were shown in Figure 14. Our sub-solar $[O/Fe]$ values are shared by clusters at similar Galactocentric distances that have been reported in other studies. Clusters with $R_{\text{GC}} > 10 \text{ kpc}$, and possibly those with $R_{\text{GC}} < 7.5 \text{ kpc}$, exhibit solar $[O/Fe]$ ratios.

Contribution of OCs to the Galactocentric radial abundance gradient has been studied by many authors for several decades. First Twarog et al. (1997) showed that there is a sharp discontinuity of the $[Fe/H]$ distribution at $R_{\text{GC}} = 10 \text{ kpc}$, which appeared to be the transition region between the inner and outer Galactic disc. Later studies, such as Yong et al. (2005) and Jacobson et al. (2009b, 2011b), concluded that the transition region lies at $R_{\text{GC}} \approx 12\text{--}14 \text{ kpc}$ by analyzing the abundances of more distant OCs. The behavior of $[O/Fe] - R_{\text{GC}}$ variation is complicated by data incompleteness. There are two more OCs we did not include in Figure 15 at 16.4 kpc (Be 20) and 22.9 kpc (Be 29) with

supersolar O abundances, $[O/Fe] = +0.18$ and $+0.23$, respectively (Yong et al. 2005). In general the distribution of $[O/Fe]$ with Galactocentric distance is not clear, scattering from -0.25 to $+0.20$, and more results for clusters far from the solar circle are needed.

Finally, Lebzelter et al. (2015) investigated the oxygen isotopic ratios in intermediate-mass giants, estimating $^{16}O/^{17}O$ and $^{16}O/^{18}O$ ratios in six red giant members of selected relatively nearby open clusters with known main sequence turnoff masses. They obtained high-resolution H and K-band spectra of these targets and used several OH lines to measure the $[^{16}O/H]$ abundances in these giants. They found an average subsolar value, $[^{16}O/H] = -0.25 \pm 0.03$ for their sample. They concluded that the initial ^{16}O abundance in the protostellar cloud is directly related to the final observed deficiency in oxygen in RG's, which can only be achieved with models have initially subsolar ^{16}O values.

7.3 Na

Na abundances show different behaviours in each cluster in our sample. While RGs of the NGC 6940 and Hyades open clusters indicate Na overabundances, NGC 752 members have approximately solar Na abundances (Paper 1). Smiljanic (2012) determined Na contents in three Hyades giants, δ Tau, ε Tau and γ Tau, and found an average non-LTE corrected $[Na/Fe] = +0.3$ dex; this is about 0.1 dex higher than what we have found in this study. The Na lines used for the abundance determination in both studies are the same (including gf values) except for the 5682.6 Å line, which was excluded by Smiljanic (2012) due to a Cr I blend. Eventually they used only 6154.2 and 6160.8 Å lines to compute the Na abundances. As reported in Takeda et al. (2003), the 6154 and 6161 Å lines are insignificantly affected by the departures from the LTE (≤ 0.1 dex) and 5683 Å line is somewhat affected for metal-poor stars with $-3 \leq [Fe/H] \leq -1$. By taking into account the contamination from Cr I blend, we found that this line gives Na abundances well in agreement with those obtained from 6154.2 and 6160.8 Å lines. The discrepancy of about 0.1 dex in Na abundance between our and Smiljanic's results may be due to slightly different $[Fe/H]$ and $\log \epsilon(Na)_{\odot}$ values in both studies. Overall, our findings seem to be well in agreement with the non-LTE results from Smiljanic (2012).

We also observe some enhancement in Na among the RGs of NGC 6940; the cluster mean is $\langle [Na/Fe] \rangle = 0.11 \pm 0.13$ dex. The high standard deviation is mainly due to MMU 108 and MMU 152, which have relatively high Na abundances of ~ 0.3 dex and ~ 0.4 dex, respectively. We also point out the modest Al overabundance in MMU 108 and MMU 152 by about 0.14 dex. These members are also enriched in N by about 0.35 dex, which is above the average of the cluster. Although overabundances in Na, Al and N abundances mimic the classic $[Na/Fe]$ - $[Al/Fe]$ and $[Na/Fe]$ - $[N/Fe]$ correlations observed in globular clusters (e.g. Kraft 1994 and references therein), this phenomenon is not common among open clusters and future investigation of a larger sample should be pursued for a definite conclusion on the distinction of NGC 6940.

Na overabundances in both NGC 6940 and Hyades may be explained by evolutionary models. Charbonnel & Lagarde (2010) investigated the effects

of different mixing scenarios for solar metallicity stars of low- and intermediate mass (1 to 4 M_{\odot}). They compared theoretical results with observational data from open cluster studies and concluded that no change in Na abundance is expected for stars with turn-off masses nearly up to 2 M_{\odot} , but for higher masses one should expect to see Na abundances enhanced by about 0.2 dex (see also Karakas & Lattanzio 2014). In the case of NGC 6940 ($M_{TO} \simeq 2 M_{\odot}$) and Hyades ($M_{TO} \simeq 2.3 M_{\odot}$), we see Na abundances enhanced by about 0.1 and 0.2 dex, respectively. Comparison of our $[Na/Fe]$ values with turn-off masses (Figure 21 in Charbonnel & Lagarde 2010) of the clusters suggests that different extra-mixing mechanisms must have been involved in each cluster. According to theoretical models of Charbonnel & Lagarde, younger open cluster Hyades shows consistency with the model predictions that include both thermohaline (th) and rotation-induced mixing (V_{ZAMS}); “th+ $V_{ZAMS}=110 \text{ km s}^{-1}$ ” and “th+ $V_{ZAMS}=250 \text{ km s}^{-1}$ ” (Figure 21 in Charbonnel & Lagarde 2010). Most of the RGs of older NGC 6940, on the other hand, coherent with the standard predictions. However, with the enhanced Na abundances, MMU 108 and MMU 152 seem to diverge from the rest of the cluster members, suggesting that these two stars share a different evolution history probably with much higher initial velocities. NGC 752 ($M_{TO} \simeq 1.6 M_{\odot}$, Paper 1) has an average Na abundance of about solar and matches well with the standard theory without the need of any additional mixing mechanisms.

Overall evaluation of the atmospheric parameters, LiCNO and Na abundances and $^{12}C/^{13}C$ ratios of the NGC 6940 RGs along with the theoretical predictions discussed above reveals that the stars in our sample are probable RC stars and were subjected to different amount/type of extra-mixing mechanisms depending on their initial masses.

This is the first extended chemical abundance analysis of the open cluster NGC 6940. Further investigation of the same members in the infrared H- and K-band spectral region using Immersion Grating Infrared Spectrograph (IGRINS; Yuk et al. 2010) is underway.

ACKNOWLEDGMENTS

We thank our referee for very helpful discussions that helped improving our paper. We also thank Craig Wheeler for helpful comments. Our work has been supported by The Scientific and Technological Research Council of Turkey (TÜBİTAK, project No. 112T929), by the US National Science Foundation (NSF, grant AST 12-11585), and by the University of Texas Rex G. Baker, Jr. Centennial Research Endowment. This research has made use of: NASA's Astrophysics Data System Bibliographic Services; the SIMBAD database and the VizieR service, both operated at CDS, Strasbourg, France; the WEBDA database, operated at the Department of Theoretical Physics and Astrophysics of the Masaryk University; and the VALD database, operated at Uppsala University, the Institute of Astronomy RAS in Moscow, and the University of Vienna.

REFERENCES

- Allende Prieto C., Lambert D. L., Asplund M., 2001, *ApJL*, 556, L63
- Asplund M., Grevesse N., Sauval A. J., Scott P., 2009, *ARA&A*, 47, 481
- Biazzo K., Frasca A., Catalano S., Marilli E., 2007a, *Astron. Nachr.*, 328, 938
- Biazzo K. et al., 2007b, *A&A*, 475, 981
- Blanco-Cuaresma S. et al., 2015, *A&A*, 577, A47
- Böcek Topcu G., Afşar M., Schaeuble M., Sneden C., 2015, *MNRAS*, 446, 3562
- Bressan A., Marigo P., Girardi L., Salasnich B., Dal Cero C., Rubele S., Nanni A., 2012, *MNRAS*, 427, 127
- Brooke J. S. A., Ram R. S., Western C. M., Li G., Schwenke D. W., Bernath P. F., 2014, *ApJS*, 210, 23
- Brugamyer E., Dodson-Robinson S. E., Cochran W. D., Sneden C., 2011, *ApJ*, 738, 97
- Cameron L. M., 1985, *A&A*, 147, 39
- Cannon R. D., 1970, *MNRAS*, 150, 111
- Carrera R., Pancino E., 2011, *A&A*, 535, A30
- Castelli F., Kurucz R. L., 2003, in N. Piskunov, W.W. Weiss, D.F. Gray, eds, *Modelling of Stellar Atmospheres*. IAU Symposium, Vol. 210, p. 20P
- Caughlan G. R., 1965, *ApJ*, 141, 688
- Charbonnel C., Lagarde N., 2010, *A&A*, 522, A10
- Cunha K., Smith V. V., Suntzeff N. B., Norris J. E., Da Costa G. S., Plez B., 2002, *AJ*, 124, 379
- Cutri R. M. et al., 2003, *VizieR Online Data Catalog*, 2246, 0
- Day R. W., Lambert D. L., Sneden C., 1973, *ApJ*, 185, 213
- Dearborn D. S. P., Eggleton P. P., Schramm D. N., 1976, *ApJ*, 203, 455
- Demarque P., Woo J. H., Kim Y. C., Yi S. K., 2004, *ApJS*, 155, 667
- Den Hartog E. A., Ruffoni M. P., Lawler J. E., Pickering J. C., Lind K., Brewer N. R., 2014, *ApJS*, 215, 23
- Dias W. S., Alessi B. S., Moitinho A., Lépine J. R. D., 2002, *A&A*, 389, 871
- Dias W. S., Monteiro H., Caetano T. C., Lépine J. R. D., Assafin M., Oliveira A. F., 2014, *A&A*, 564, A79
- Dotter A., Chaboyer B., Jevremović D., Kostov V., Baron E., Ferguson J. W., 2008, *ApJS*, 178, 89
- Drazdauskas A., Tautvaišienė G., Randich S., Bragaglia A., Mikolaitis Š., Janulis R., 2016, *A&A*, 589, A50
- Fitzpatrick M. J., 1993, in R.J. Hanisch, R.J.V. Brissenden, J. Barnes, eds, *Astronomical Data Analysis Software and Systems II*. Astronomical Society of the Pacific Conference Series, Vol. 52, p. 472
- Friel E. D., Jacobson H. R., Pilachowski C. A., 2005, *AJ*, 129, 2725
- Friel E. D., Jacobson H. R., Pilachowski C. A., 2010, *AJ*, 139, 1942
- Friel E. D., Janes K. A., Tavares M., Scott J., Katsanis R., Lotz J., Hong L., Miller N., 2002, *AJ*, 124, 2693
- Geisler D., 1988, *PASP*, 100, 338
- Gilroy K. K., 1989, *ApJ*, 347, 835
- Gilroy K. K., Brown J. A., 1991, *ApJ*, 371, 578
- Gray D. F., Brown K., 2001, *PASP*, 113, 723
- Gray D. F., Johanson H. L., 1991, *PASP*, 103, 439
- Grevesse N., Sauval A. J., 1998, *Space Sci. Rev.*, 85, 161
- Grevesse N., Asplund M., Sauval A. J., 2007, *Space Sci. Rev.*, 130, 105
- Hannaford P., Lowe R. M., 1983, *Optical Engineering*, 22, 532
- Hartwick F. D. A., McClure R. D., 1972, *PASP*, 84, 288
- Hinkle K., Wallace L., Valenti J., Harmer D., 2000, *Visible and Near Infrared Atlas of the Arcturus Spectrum 3727-9300 Å*
- Hoag A. A., Johnson H. L., Iriarte B., Mitchell R. I., Hallam K. L., Sharpless S., 1961, *Publications of the U.S. Naval Observatory Second Series*, 17, 343
- Hog E., Kuzmin A., Bastian U., Fabricius C., Kuimov K., Lindegren L., Makarov V. V., Roeser S., 1998, *A&A*, 335, L65
- Høg E. et al., 2000, *A&A*, 355, L27
- Iben Jr. I., 1967, *ApJ*, 147, 624
- Jacobson H. R., Friel E. D., Pilachowski C. A., 2008, *AJ*, 135, 2341
- Jacobson H. R., Friel E. D., Pilachowski C. A., 2009a, *AJ*, 137, 4753
- Jacobson H. R., Friel E. D., Pilachowski C. A., 2009b, *AJ*, 137, 4753
- Jacobson H. R., Pilachowski C. A., Friel E. D., 2011a, *AJ*, 142, 59
- Jacobson H. R., Pilachowski C. A., Friel E. D., 2011b, *AJ*, 142, 59
- Jennens P. A., Helfer H. L., 1975, *MNRAS*, 172, 681
- Johansson S., Litzén U., Lundberg H., Zhang Z., 2003, *ApJL*, 584, L107
- Johnson H. L., Knuckles C. F., 1955, *ApJ*, 122, 209
- Johnson H. L., Hoag A. A., Iriarte B., Mitchell R. I., Hallam K. L., 1961, *Lowell Observatory Bulletin*, 5, 133
- Kaempf T. A., de Boer K. S., Altmann M., 2005, *A&A*, 432, 879
- Karakas A. I., Lattanzio J. C., 2014, *PASA*, 31, e030
- Kharchenko N. V., Piskunov A. E., Röser S., Schilbach E., Scholz R. D., 2005, *A&A*, 438, 1163
- Kraft R. P., 1994, *PASP*, 106, 553
- Kurucz R. L., Furenlid I., Brault J., Testerman L., 1984, *Solar flux atlas from 296 to 1300 nm*. National Solar Observatory Atlas, Sunspot, New Mexico: National Solar Observatory, 1984
- Lambert D. L., Ries L. M., 1981, *ApJ*, 248, 228
- Larsson-Leander G., 1960, *Stockholms Observatoriums Annaler*, 20, 9
- Larsson-Leander G., 1964, *ApJ*, 140, 144
- Lawler J. E., Wood M. P., Den Hartog E. A., Feigenson T., Sneden C., Cowan J. J., 2014, *ApJS*, 215, 20
- Lawler J. E., Sneden C., Cowan J. J., 2015, *ApJS*, 220, 13
- Lebzelter T., Straniero O., Hinkle K. H., Nowotny W., Aringer B., 2015, *A&A*, 578, A33
- Liu F., Yong D., Asplund M., Ramírez I., Meléndez J., 2016, *MNRAS*, 457, 3934
- Lobel A., 2011, *Can. J. Phys.*, 89, 395
- Loktin A. V., Gerasimenko T. P., Malysheva L. K., 2001, *Astronomical and Astrophysical Transactions.*, 20, 607
- Luck R. E., 1994, *ApJS*, 91, 309
- Lynga G., 1995, *VizieR Online Data Catalog*, 7092, 0
- Maderak R. M., Deliyannis C. P., King J. R., Cummings J. D., 2013, *AJ*, 146, 143
- Malysheva L. K., 1997, *Astronomy Letters.*, 23, 585
- Masseron T. et al., 2014, *A&A*, 571, A47
- Mathieu R. D., 2000, in R. Pallavicini, G. Micela,

- S. Sciortino, eds, *Stellar Clusters and Associations: Convection, Rotation, and Dynamos*. Astronomical Society of the Pacific Conference Series, Vol. 198, p. 517
- Mermilliod J. C., Mayor M., 1989, *A&A*, 219, 125
- Mermilliod J. C., Mayor M., Udry S., 2008, *A&A*, 485, 303
- Mikolaitis Š., Tautvaišienė G., Gratton R., Bragaglia A., Carretta E., 2010, *MNRAS*, 407, 1866
- Mikolaitis Š., Tautvaišienė G., Gratton R., Bragaglia A., Carretta E., 2011a, *MNRAS*, 413, 2199
- Mikolaitis Š., Tautvaišienė G., Gratton R., Bragaglia A., Carretta E., 2011b, *MNRAS*, 416, 1092
- Mikolaitis Š., Tautvaišienė G., Gratton R., Bragaglia A., Carretta E., 2012, *A&A*, 541, A137
- O'Brian T. R., Wickliffe M. E., Lawler J. E., Whaling W., Brault J. W., 1991, *J. Opt. Soc. Am. B*, 8, 1185
- Palmerini S., Cristallo S., Busso M., Abia C., Uttenthaler S., Gialanella L., Maiorca E., 2011, *ApJ*, 741, 26
- Pancino E., Carrera R., Rossetti E., Gallart C., 2010, *A&A*, 511, A56
- Paulson D. B., Sneden C., Cochran W. D., 2003, *AJ*, 125, 3185
- Perryman M. A. C. et al., 1998, *A&A*, 331, 81
- Ramírez I., Meléndez J., 2005, *ApJ*, 626, 465
- Reddy A. B. S., Lambert D. L., 2016, *A&A*, 589, A57
- Roederer I. U., Sneden C., Thompson I. B., Preston G. W., Shectman S. A., 2010, *ApJ*, 711, 573
- Ruffoni M. P., Den Hartog E. A., Lawler J. E., Brewer N. R., Lind K., Nave G., Pickering J. C., 2014, *MNRAS*, 441, 3127
- Ryabchikova T., Piskunov N., Kurucz R. L., Stempels H. C., Heiter U., Pakhomov Y., Barklem P. S., 2015, *Physica Scripta*, 90, 054005
- Sanders W. L., 1972, *A&A*, 16, 58
- Santrich O. J. K., Pereira C. B., Drake N. A., 2013, *A&A*, 554, A2
- Schuler S. C., Hatzes A. P., King J. R., Kürster M., The L. S., 2006, *AJ*, 131, 1057
- Schuler S. C., King J. R., The L. S., 2009, *ApJ*, 701, 837
- Smiljanic R., 2012, *MNRAS*, 422, 1562
- Smiljanic R., Gauderon R., North P., Barbuy B., Charbonnel C., Mowlavi N., 2009, *A&A*, 502, 267
- Smiljanic R. et al., 2016, *A&A*, 589, A115
- Sneden C., 1973, *ApJ*, 184, 839
- Sneden C., Lucatello S., Ram R. S., Brooke J. S. A., Bernath P., 2014, *ApJS*, 214, 26
- Stetson P. B., 2000, *PASP*, 112, 925
- Strassmeier K. G., Schordan P., 2000, *Astron. Nachr.*, 321, 277
- Strobel A., 1991a, *A&A*, 247, 35
- Strobel A., 1991b, *Astronomische Nachrichten*, 312, 177
- Tagliaferri G., Belloni T., 1997, *Mem. Societa Astronomica Italiana*, 68, 1001
- Takeda Y., Zhao G., Takada-Hidai M., Chen Y. Q., Saito Y. J., Zhang H. W., 2003, *Chin. J. Astron. Astrophys.*, 3, 316
- Tautvaišienė G., Edvardsson B., Tuominen I., Ilyin I., 2000, *A&A*, 360, 499
- Tautvaišienė G., Edvardsson B., Tuominen I., Ilyin I., 2001, *A&A*, 380, 578
- Tautvaišienė G., Edvardsson B., Puzeras E., Ilyin I., 2005, *A&A*, 431, 933
- Tautvaišienė G. et al., 2015, *A&A*, 573, A55
- Thogersen E. N., Friel E. D., Fallon B. V., 1993, *PASP*, 105, 1253
- Tomkin J., Luck R. E., Lambert D. L., 1976, *ApJ*, 210, 694
- Torres G., 2010, *AJ*, 140, 1158
- Trumpler R. J., 1930, *Lick Observatory Bulletin*, 14, 154
- Tull R. G., 1998, in S. D'Odorico, ed., *Optical Astronomical Instrumentation*. Society of Photo-Optical Instrumentation Engineers (SPIE) Conference Series, Vol. 3355, pp. 387–398
- Tull R. G., MacQueen P. J., Sneden C., Lambert D. L., 1995, *PASP*, 107, 251
- Twarog B. A., Ashman K. M., Anthony-Twarog B. J., 1997, *AJ*, 114, 2556
- van den Bergh S., McClure R. D., 1980, *A&A*, 88, 360
- Vasilevskis S., Rach R. A., 1957, *AJ*, 62, 175
- Walker M. F., 1958, *ApJ*, 128, 562
- Weidemann V., Jordan S., Iben Jr. I., Casertano S., 1992, *AJ*, 104, 1876
- Yong D., Carney B. W., Teixeira de Almeida M. L., 2005, *AJ*, 130, 597
- Yuk I. S. et al., 2010, in *Society of Photo-Optical Instrumentation Engineers (SPIE) Conference Series*. Society of Photo-Optical Instrumentation Engineers (SPIE) Conference Series, Vol. 7735, p. 1
- Začs L., Alksnis O., Barzdis A., Laure A., Musaev F. A., Bondar A., Sperauskas J., 2011, *MNRAS*, 417, 649